UvA-DARE (Digital Academic Repository)

Finite representation of reaction kinetics in unbounded biopolymer structures

Orlova, Y.; Gambardella, A.A.; Harmon, R.E.; Kryven, I.; Iedema, P.D.

Link to publication

Finite representation of reaction kinetics in unbounded biopolymer structures

Yuliia Orlova[a], Alessa A. Gambardella[b], Rebecca E. Harmon[a,c], Ivan Kryven[d,e,*], Piet D. Iedema[a]

[a] *University of Amsterdam, Van 't Hoff Institute for Molecular Sciences, Amsterdam 1098 XH, The Netherlands*
[b] *Rijksmuseum, Amsterdam 1071 ZC, The Netherlands*
[c] *Northwestern University, Department of Chemical and Biological Engineering, Evanston, IL 60208, USA*
[d] *Mathematical Institute, Utrecht University, Utrecht 3584 CD, The Netherlands*
[e] *Centre for Complex Systems Studies, 3584 CE Utrecht, The Netherlands*

HIGHLIGHTS

- Automated reaction network generation is applied to model complex polymerisation.
- Concentrations of functional groups are obtained from a kinetic model.
- Random graphs are used to infer properties of soluble fractions of the material.
- Concentrations of monomers and dimers are validated with ESI-MS measurements.

ARTICLE INFO

ABSTRACT

Several systems in organic chemistry are so large and complex that formulating the rate equations for their kinetics is difficult. Examples include polymerization of bio-derived materials, such as natural oils and resins, and metabolic oxidation reactions, as in the Krebs cycle. The challenge lies in the diversity of reaction products and their growth in size, which may be unbounded due to the polymerization-like reactions. Here we demonstrate an algorithm that formulates the kinetics of chemical systems of unlimited size in terms of a fine number of fragment species, and therefore, renders such structures tractable for kinetic modelling. We study a complex system of ethyl linoleate polymerization using such an algorithm. Additionally, we show that the algorithm may assist interpreting experimental measurements from electrospray ionization mass spectrometry.

1. Introduction

Simply defined design tasks, such as synthesis planning [1,2], often involve a large number of choices. In the present paper, we address a problem of formulating a large system of ordinary differential equations (ODEs) that implements autoxidation reaction kinetics of a bio-based polymer. Constructing such a system poses a challenge due to a large number of possible reaction pathways and growing number of species that soon becomes computationally intractable. This means that we do not possess *a priori* knowledge of the underlying reaction network, and that such a network may eventually appear too large to be represented in full on a computer. This paper explores algorithms for *automated reaction network generation (ARNG)* to overcome the aforementioned challenges.

The ARNG concept was introduced in the works by Yoneda [3] and

Clymans and Froment [4], and was later adapted to handle a wide range of chemical systems [5–11]. ARNG was applied to metabolic processes [12,13], prebiotic scenarios [14], protein interaction exploration [15–18], pharmaceutical design [19] and design of regulation for cell functions [20]. Oakley et al. [21,22] addressed the drying process of ethyl linoleate by limiting their study to hexamers as the largest oligomer. This approach proved to be sufficient in capturing the early stage of polymerization, however an infinite growth of molecules during polymerization still remains an open problem in the context of ARNG. In our recent ARNG algorithm [23], a polymer is thought to be fragmented into a finite number of monomer structures, and the reaction network is formulated in terms of the latter species. Such a fragmentation approach is inspired by polymer reaction engineering [24–26] and allows one to obtain a finite system of ODEs describing reaction kinetics of a virtually infinite polymer, as we operate with

reactions that act on small structures rather than on the entire polymer. In the present work we demonstrate that much of the information about the structure of the whole polymer can nevertheless be inferred using the concept of *random graphs* [27–31].

We explore the polymerization of ethyl linoleate (EL) by formulating the reaction network for monomer fragments and further transforming it into a system of ODEs for species concentrations. In this chemical process, many reactions occur simultaneously leading to the formation of a wide range of intermediate products that ultimately become the monomeric constituents of an infinite polymer network [32,33]. We present evolution profiles of selected byproducts of such reactions, such as: alcohols, peroxides, aldehydes, carboxylic acids, and epoxides. We also report the properties of soluble polymeric fractions, such as the buildup of the average molecular weight and the distribution of molecular sizes. Alongside, we calculate the masses of all explicit monomers and dimers, which are reconstructed as combinations of monomer fragments. The latter information aids interpreting the mass spectrum obtained with electrospray ionization mass spectrometry (ESI-MS) of EL, as the model provides mass data that are comparable to the measurements [34].

Polymerization of ethyl linoleate (EL) is an accepted model system for the autoxidative drying process of linseed oil under the influence of light and oxygen. Understanding the kinetics of autoxidative drying of linseed oil is relevant to oil paint characterization and design of preservation techniques for ageing oil paintings [35–39]. Our study also contributes to the conservation of oil paintings by providing a better understanding of the binding medium structure as it evolves from the fresh condition to heavily degraded states. For instance, our model describes the influence of a drier, commonly added to accelerate drying, on the rate of formation of all investigated functional groups in different temperature regimes. Surprisingly, the model also predicts long-lasting effects of the drier on the structural properties of the ethyl linoleate polymer.

2. Materials and methods

2.1. Reaction mechanism – database

The chemistry of the photo-oxidative drying process of linseed oil and associated model systems, such as EL, has been thoroughly studied by experimental research, particularly in the context of binding media of oil paint [40–43]. While exploring various aspects of drying (drying rate, emission of volatile compounds), a better understanding of elementary reaction steps of the autoxidation process has been achieved. Studies regarding drier influence on autoxidation of EL and linseed oil have been performed [44–49]. In these studies, concentration profiles of peroxides, oxygen uptake and production of small volatile compounds are reported. Reviews exist [46,50–52] that provide detailed descriptions of the autoxidation reaction mechanism that in part go back to many studies of the organic chemistry of lipid autoxidation by the group of Porter et al. [53–56]. Work by Muizebelt et al. [57] provides insights on how relative amounts of bis-allylic carbons, conjugated double bonds, epoxides, acids, peroxy and ether crosslinks evolve over time. Emission of volatile compounds, such as hexanal and pentanal, during the oxidation of EL are measured and reported in studies by Oakley et al. [58] and others [51,59]. These references form a database for a complete chemical description of the EL case study; they are also employed to validate the outcomes of the resulting kinetic model.

We adopt the usual way of representing reactions in organic chemistry by listing the structural formulas and show some of the most important reaction steps in Fig. 1. The polymerization starts with the abstraction of hydrogen from bis-allylic carbon. The carbon radical reacts with molecular oxygen and forms a peroxy radical. Peroxy radicals form hydroperoxides by abstracting more hydrogens from bis-allylic carbons. Under the influence of UV light or a metal drier,

hydroperoxides dissociate into alkoxy and peroxy radicals. Alkoxy radicals are also active in hydrogen abstraction. Alkoxy, peroxy and carbon radicals actively undergo termination by recombination forming ether, peroxy and alkyl crosslinks, respectively. Additionally, termination by disproportionation between two peroxy radicals, also known as Russell termination, produces ketones and alcohols. In the addition reaction the peroxy radical connects to one of the carbon atoms with conjugated double bonds, forming a peroxy crosslink. Note that this reaction type is the dominant propagation reaction in radical polymerization, where the radical undergoes either propagation or termination reactions in competition. It should be noted that Fig. 1 by no means represents the whole reaction network, but only a small fragment of it, preceding actual polymer.

We describe two more reactions, β-scission and epoxide formation. β-scission is thought to be responsible for the formation of volatile aldehydes [50,60] according to several mechanisms. As shown in Fig. 1, we account for two pathways. Pathway 1 starts with an alkoxy radical located near a conjugated double bond. Scission takes place at the carbon connected to the oxygen radical leading to an aldehyde fragment with a conjugated double bond and R2, and a fragment R1'. Pathway 2 has been proposed by Oakley et al. [60] and presumes the existence of an alkoxy radical near a peroxy crosslink and a singular double bond. This species is a product of an addition reaction and its β-scission leads to an aldehyde fragment with R2 and a fragment with a peroxy crosslink and R1. In addition, two pathways leading to the epoxide formation have also been included in the reaction scheme [58].

2.2. Automated reaction network generator

ARNG is a methodology designed for an algorithmic reconstruction of complex reaction mechanisms. This methodology is applicable to chemical systems involving a large number of intermediate and product species. Reconstructing such reaction networks manually is virtually impossible. A number of software packages [61] have been developed for automatic generation of reaction networks for various types of chemistry. Here, we will discuss several important concepts of such methodology.

In ARNG, molecules are represented as molecular graphs [62,63]. A graph is a mathematical object that consists of nodes connected by edges. A direct analogy between molecules and graphs can be easily understood: atoms are nodes and edges represent the bonds between atoms. A node is assigned a label corresponding to an atom and an edge has a weight corresponding to the bond order. Graphs are usually represented by their adjacency matrix (or adjacency list) and a list of labels for the nodes. This notation is further extended by indicating the number of unpaired electrons, or radicals, on the diagonal of the adjacency matrix. The molecular graph of the initial state of EL is shown in Fig. 2 a.

Describing reactions requires defining transformations of molecular graphs representing the change of a reactant into a product. For this purpose, we define a 'pattern' to be a reactive part of a molecule. The idea of patterns has been employed before in the field of synthesis planning [64]. In terms of a graph representation, a pattern is a subgraph of a molecular graph that undergoes changes due to a reaction. A reaction is defined as a transformation applied to a reactant pattern and resulting in a product pattern. In a large chemical system one molecule may consist of more than one pattern, which implies that it can undergo changes according to more than one reaction pathway. Furthermore, the same pattern may appear repeatedly during different 'states' that a monomer unit is passing through during the chain of transformations. As a consequence, a limited set of reaction rules suffices to define a reaction mechanism, although the repeated application of these rules will still result in many reactions between various states of the molecules. In the ARNG methodology we defined patterns manually and did not employ a method that utilizes machine learning techniques to extract patterns and reaction rules from large chemical databases [65].
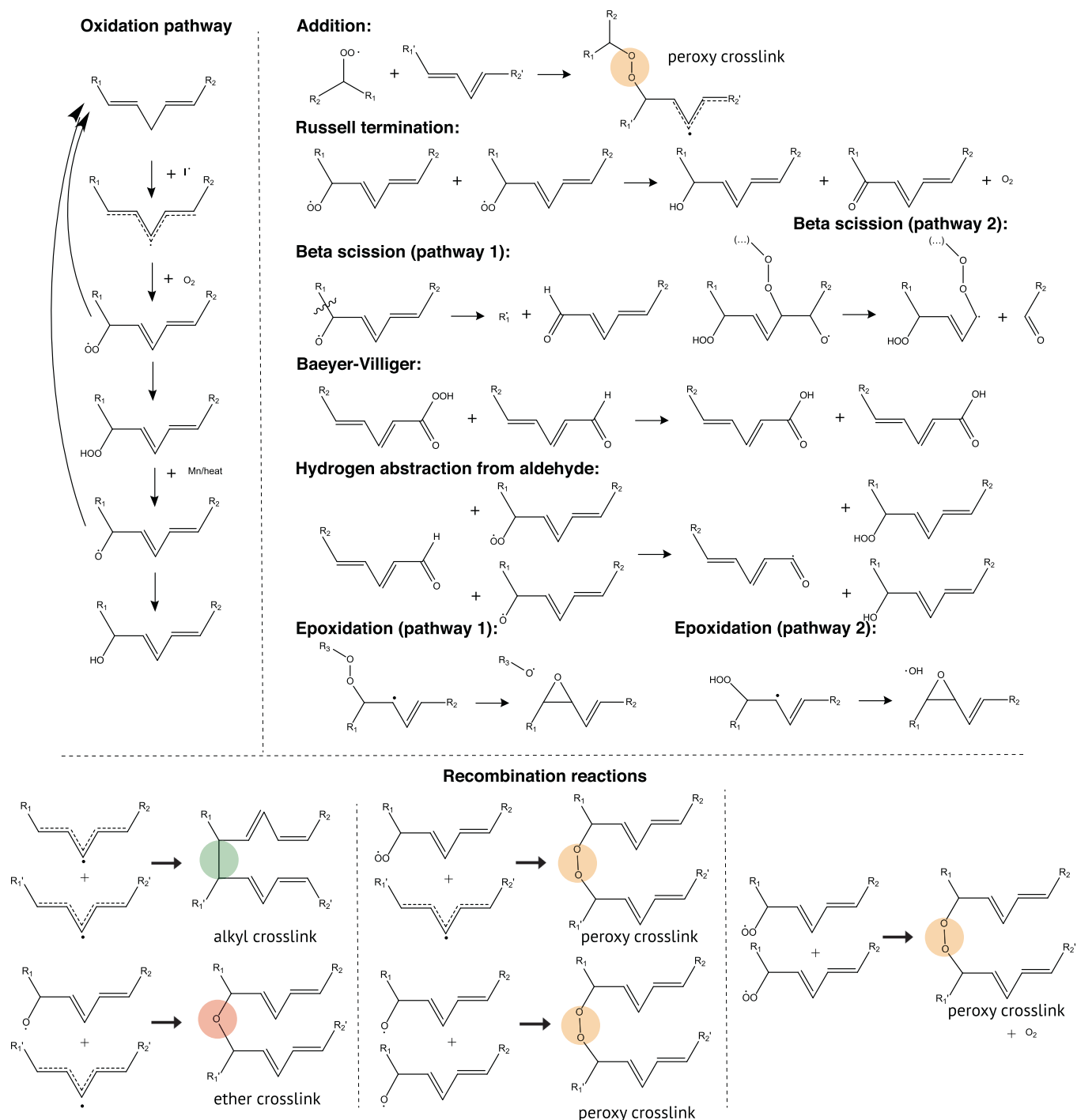
Fig. 1. Schematic representation of the reaction steps occurring during the polymerization of ethyl linoleate. Different types of crosslinks are possible: alkyl crosslink (highlighted in green) formed via the recombination of two carbon radicals, ether crosslink (highlighted in red) formed via the recombination of carbon radical and alkoxy radical, peroxy crosslink (highlighted in orange) formed via recombination of peroxy radical and carbon radical, recombination of two alkoxy radicals or via addition reaction. (For interpretation of the references to colour in this figure legend, the reader is referred to the web version of this article.)

To initialize the ARNG one needs to define the reaction rules and construct the molecular graph of an initial state of the molecule of interest. Furthermore, the algorithm scrutinizes the reactive sites of each discovered molecule and applies transformations to them according to the reaction rules. Such transformations result in new molecular states that expand the list of molecules available for the reactions. Every time a molecule is created, it is compared to all existing molecular structures. If the molecule is not already in the list of previously created molecules, it is enlisted as a new molecular species. Consecutively applying reaction rules to newly generated molecules allows to reconstruct the

reaction network of all possible molecular states that may appear under the given conditions and reaction rules. Finally, all the transformations uncovered are assembled into a reaction network – a bipartite graph that captures all the interactions between reconstructed molecular states. The adjacency matrix representing the reaction network is then used to automatically construct the rate equations for the species concentrations[23]. Calculation of the rate coefficients is described in the following subsection. The main steps of ARNG algorithm are shown as a flow-chart in Fig. 2 b.

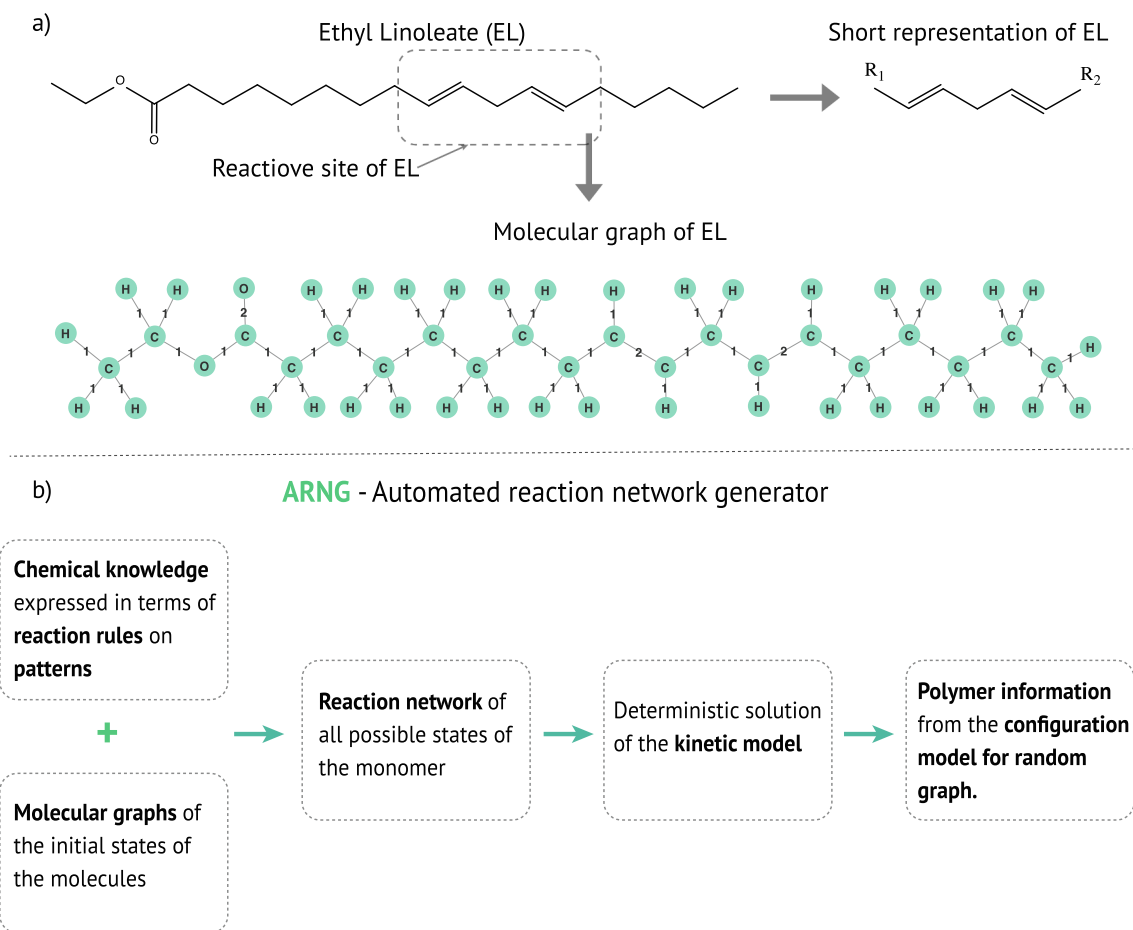We assume the pre-exponential factor, intrinsic energy and transfer

a)

Ethyl Linoleate (EL)

Short representation of EL

Reactiove site of EL

Molecular graph of EL

b)

ARNG - Automated reaction network generator

Fig. 2. (a) Chemical structure of EL (reactive site is highlighted) and its representation as a molecular graph. (b) The scheme that describes the key steps in ARNG.

coefficient to be the same within a reaction family, and we take these values from the literature. However, heat of reaction is the value that we calculate for each reaction individually. Heat of reaction is the difference between enthalpy of products and enthalpy of reactants, where enthalpy of formation for each molecular structure can be estimated using the group additivity principle. Thus, the heat of reaction is the value that is calculated for each reaction individually. However, there are some reactions, like cobalt chemistry, for which the pre-exponential factor, intrinsic energy and coefficient α are not available in the literature. For these reactions, we indeed use rate coefficients from the literature. It is a valid point to mention, and we adjusted the text in the "Rate parameters" subsection accordingly.

2.3. Rate parameters

Since using experimental rates or state-of-the-art estimation techniques (i.e. quantum chemical calculations) for each rate coefficient is virtually impossible in view of the vast number of elementary reaction steps in a complex reaction network, we estimate the kinetic parameters of the model using the concept of 'reaction families' [66,67] with a procedure from Oakley et al. [58]. Rate coefficients for the reaction families involving cobalt chemistry are taken directly from the literature, as there are no parameters available to calculate them for each individual reaction. The rates coefficients of other reaction families are calculated for each elementary reaction by the Arrhenius equation,

$$k = A exp(-E_a/RT).$$

The activation energy, E_a, is approximated using the Evans-Polanyi structure-reactivity relationship for each reaction family. The relationship relates enthalpy of reaction, H_{rxn}, to activation energy by

$$E_a = E_0 + \alpha \Delta H_{rxn},$$

where E_0 is the intrinsic energy barrier and α is the transfer coefficient which describes how 'reactant-like' or 'product-like' the transition-state is [68]. The forward and reverse reaction transfer coefficients sum to 1 and share an intrinsic kinetic barrier, E_0. The frequency factors of reactions of a given family are roughly entropically consistent, so a representative A may be derived from theory for that family. Additionally, the frequency factors of forward and reverse reaction pairs are thermodynamically consistent related to the change in free energy. In this work, we assume irreversibility of reactions resulting in products, which are known to be stable at the low temperatures, namely: alcohol, carbonyl and carboxyl groups, as well as alkyl and ether crosslinks. Among reactions that form such groups are: recombination between alkyl and alkoxyl radicals, Russell termination and Baeyer-Villiger reaction. This simplifying assumption allows restricting the size of a model, although a more rigorous model should be able to tackle the reversibility of all reactions. Both, computer and lab experiments have been used to determine the values of A and E_0 for each reaction family [69,70]. A list of reaction families with parameter values is given in Table 1. We assume the pre-exponential factor A, intrinsic energy E_0 and transfer coefficient α to be the same within a reaction family, and we take these values from the literature. However, heat of reaction is the value that we calculate for each reaction individually.

The heat of reaction for each unique elementary step is calculated from the difference between the product and reactant enthalpies of formation computed using Benson's thermochemical group additivity method [72]. According to this method the energy contribution of central atoms and their immediate neighbours are added up to obtain the heat of formation of a species, using published group additivity

Table 1

Kinetic parameters used in the model, values for k and A and in L/mol s for bimolecular reaction and in s^{-1} for unimolecular reaction.

Reaction family	k (293 K)	A	E_0 (kcal/mol)	α	Reference
Primary initiation: Co(II) + O₂ ⟶ Co(III) OO.	0.666 [21]	10^{13}	0	1	[69]
Secondary initiation: RH + Co(III) OO. ⟶ R. + Co(III) OOH	5 * 10^{-5} [21]				
		10^{15}	0	1	[69]
Secondary initiation (no drier mode): RH + O₂ → R. +.OOH		10^{13} 10^{19} (value used)	0	1	[69]
Co(III) OOH → Co(II) + HO2.	0.5				[21]
ROOH decomposition with catalyst ROOH + Co(II) → RO. + [Co(III) OH−]	0.5 [21]				
	0.0643 [49]				[49]
	2.7 * 10^8				
ROOH + [Co(III) OH−] → [Co(III) OOR] + H₂O	2				[21]
Co(III) OOR decomposition: [Co(III) OOR] → Co(II) + ROO	0.0095 [21]				[49]
[Co(III) OOR] + ROOH → [Co(III) OOR, HOOR]	900 [21]				[49]
[Co(III) OOR, HOOR] → RO. + [Co(III) OOR,OH]	0.0095 [21]				[49]
[Co(III) OOR,OH] → ROO. + [Co(III) OH−]	0.0095 [21]				[49]
Oxidation: R. + O₂ → ROO.	10^8	10^8	0	0	[69]
Hydrogen abstraction: RH + ROO. → R. + ROOH	6.6 [21]	10^7	3.05	1.1	[69]
Hydrogen abstraction: RH + RO. → R. + ROH		10^7	11.9	0.91	[21]
Hydrogen abstraction: RC(O) H + ROO. → RC(O). + ROOH		10^7	6.2	1	[22]
Hydrogen abstraction: RC(O) H + RO. → RC(O). + ROH		10^7	11.9	0.91	[69]
Hydrogen transfer: RH + R. → R. + RH		10^7	9.1	0.4	[21]
Hydroperoxide decomposition: ROOH → RO. + HO.		10^{15}	0	1	[69]
β-scission (see pathway 1 in Fig. 5): RO. → RC(O) H + R.		10^{14}	9.5	0.85	[60]
β-scission from dimer (see pathway 2 in Fig. 5)		10^{14}	8.7	0.85	[60]
Recombination: R. + R. → RR		10^8	R*T	0	[69]
Recombination:R. + ROO. → ROOR		10^8	R*T	0	[69]
Recombination:RO. + ROO. → ROOR		10^8	R*T	0	[69]
Recombination:R. + RO. → ROR		10^8	R*T	0	[69]
Disproportionation:ROO. + ROO. → 2RO. + O2 Russell termination: ROO. + ROO. → ROH + R(O) + O2	10^6	10^6	0	0	[58]
Addition (see Fig. 5)		10^8	11.24	0.24	[71]
ROOR decomposition: ROOR → RO. + RO. (assumed value, same as ROOH decomposition [69])		10^{15}	0	1	
Bayer Villiger:RC(O) OOH + RC(O) H → 2RC(O) OH		1.2 * 10^4	8.5	0	[69]
Epoxidation from ROOR (see pathway 1 in Fig. 5)		$10^{11.6}$	21.9	0.51	[58]
Epoxidation from ROOH (see pathway 2 in Fig. 5)		10^{13}	19.3	0.51	[58]

values from [73–77]. We use group additivity values assuming homogeneous gas phase, as the literature for condensed phase is not as rich, especially for radical centered groups and many other groups that do not have reported values or heats of vaporization to adjust final heats of reactions. Group additivity values impose an uncertainty of 0.5–1.5 kcal/mol [77] in the heat of reaction, which then influences the model coefficients and the final output of the kinetic model. In this work, we report parameter sensitivity for the families of kinetic parameters, however proper uncertainty quantification remains an open question. Analysis of the output uncertainty it is a very important question that we will separately address in our future work.

2.4. Experimental details

Paint models for study with ESI-MS were prepared with ethyl linoleate (Sigma-Aldrich) and inorganically-coated titanium dioxide (rutile form) pigment (Tronox CR-826), which was chosen for its chemical inertness towards linseed oil binding medium as compared to other pigments [78]. The method for model preparation and ageing; ESI-MS measurements; and data processing, peak picking, and matching exactly followed that reported in Orlova et al. [34].

3. Results and discussion

3.1. Algorithmic construction of the reaction network for EL

Consider, a set of distinct molecular species. All reactions that take place between the species comprise the reaction network, which is a directed bipartite graph that consists of 1) reaction nodes and 2) species nodes [79] (see Fig. 3). The reactions and species nodes have weights that correspond to the rate coefficient of a reaction and concentration of
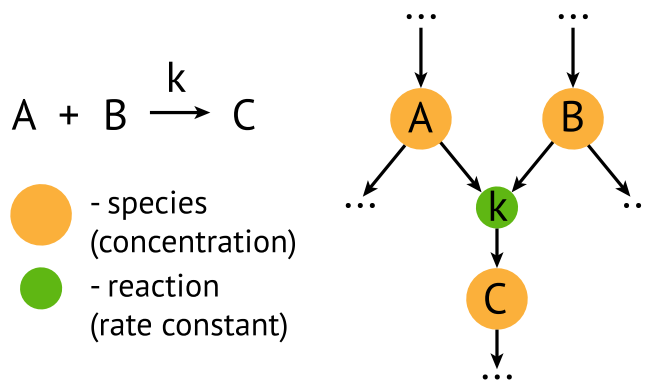
Fig. 3. Example of a reaction A + B → C with a rate coefficient k represented as a part of the reaction network. The reaction network has two types of nodes: monomer states (big orange nodes) and reactions (small green nodes). Directed edges point in the direction of a reaction: from reactant nodes to a reaction node and then from a reaction node to a product node. (For interpretation of the references to colour in this figure legend, the reader is referred to the web version of this article.)

a species, respectively. Such a network can be directly transformed into a system of ODEs for the reaction kinetics.

For simple systems, reaction networks may be formulated manually using principles of organic chemistry. For a complex system, such a EL autoxidation, formulating the reaction network can be practically done only with an algorithm due to a large size of the network. In their core, such algorithms perform multiple rounds of a subgraph isomorphism test to identify pairs of species that can react. The computational cost of this test is known to be sensitive to the sizes of the graph and the template subgraph. Due to the dependence on this test, ARNG cannot be
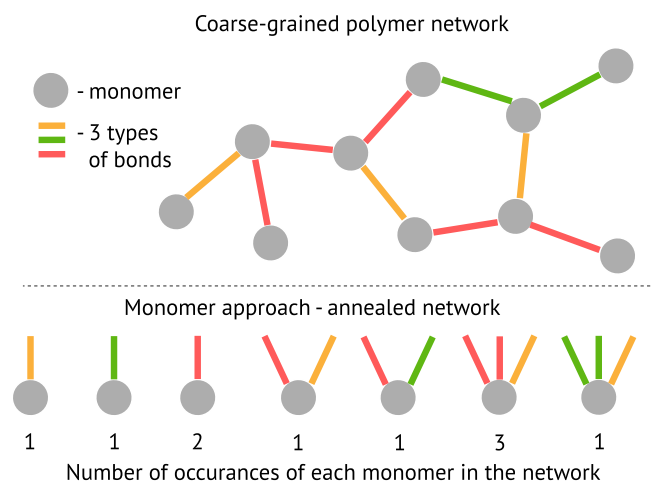
Fig. 4. The random graph representation of polymer network. Grey nodes correspond to monomers fragments, and coloured edges correspond to 3 different types of crosslinks. The network is then thought of as a an ensemble of valid wiring configurations of nodes whose connections respect the colour of half edges[31]. (For interpretation of the references to colour in this figure legend, the reader is referred to the web version of this article.)

applied to polymerization systems without a compromise. Recall that during polymerization, the size and number of chemical species continuously grows in time, and therefore, such species have virtually no bound on their size. The novelty that we introduced in our previous work [23] and further extend with approximation of the rate parameters in this work is that we formulate an ARNG algorithm acting on a special kind of a random graph. Our random graph[31] consists of a set of conventional molecular graphs, in which nodes additionally bear labelled *half-edges*. A half edge is a bond that is connected to a defined atom on one side, but has many possible candidates on the other side, and thus brings the notion of combinatorics to graph representation of molecules. This concept is illustrated in Fig. 4, where nodes are species and bonds are (half) crosslinks, and in expanded version in Fig. 2 a, where the entire atomistic molecular graph of EL is shown. The algorithm successively applies the reaction rules formulated for the subgraphs, which we call reactive patterns [64], and thus generates new species. This procedure increases the number of monomer structures until possibilities for a new reaction have been exhausted. The half crosslinks may be conserved, appear, or disappear as a result of such a transformation. As an output, the algorithm generates the list of all (fragment) species and the complete reaction network for them.

To apply the algorithm to EL, we have manually identified 74 subgraph patterns, see Appendix A, and formulated 82 reaction rules, see Appendix B, acting on such patterns that summarise reports on oil autoxidation [42,44,46,50,51,57,80] with our standardised notation. A large part of the reactions involves radicals as they are the most reactive species. We make a common assumption that multiradicals have negligible concentration, and thus exclude them from the reaction network. The final reaction network of EL polymerization consists of 3 887 fragment species and 3 444 003 reactions, and indicates that initially disconnected species gradually attain alkyl, ether, or peroxy half crosslinks as the reactions progress in time, Fig. 1. Each species bears at most three of such half crosslinks, and therefore the degree distribution has a maximum degree of three. In this work, the aim of the reaction network is to account for the formation of all stable products that are found experimentally and might play a role in paint degradation process, although their concentration might be minor. Moreover, reducing the size of reaction network by formulating it in terms of functional groups is not a straightforward task due to the presence of patterns that consist of more than one functional group (patterns 17, 24, 33–36 in Appendix A).

The entire bipartite reaction network has of the order 10^6 nodes.

Fig. 5 illustrates a projected reaction network composed solely of species nodes, with two nodes being connected with a directed edge if they participate in the same reaction as a reactant and a direct transformation product, respectively. Such an illustration allows to explore transformation pathways. In Fig. 5, the nodes are coloured according to the degree of the species they represent, that is the number of half crosslinks that the species is bearing. Such a colouring reveals nuances of the degree distribution dynamics: the nodes with the largest degree turn out to appear at the intermediate stages of the reaction pathways, that is between the centre and periphery of the network. This is a consequence of the secondary fragmentation reactions (β-scission) and relative instability of peroxy crosslinks, which are the most abundant crosslinks in the system.

3.2. Molecular species identification and Mass Spectrometry

The reaction network of EL autoxidation, as generated by the above-described procedure, captures the formation of infinitely-large molecules, while reproducing the exact structures of the fragments as molecular graphs. Such a description is complementary to the measurements by mass spectrometry (MS) [34]. The comparison is only limited to the possible *identity* of the species detected by MS with the species predicted by the algorithm.

In this work, the computational output is enhanced by the inclusion of dimers in the interpretation of the mass spectrum, as compared to our previous work [34]. The diversity in molecular species on the level of monomers and dimers is assessed by counting the number of species having zero or one half crosslink in the reaction network. When looking solely at species diversity, and not their concentration, species with zero and one half crosslink amount to 68% of all species in the reaction network, see Fig. 5. Such a variety of species is confirmed by ESI-MS measurements of the artificially aged EL sample, in positive and negative modes.

ESI-MS measurements provide experimental information about the mass distribution of the extractable material of artificially aged EL. Calculating masses of the computer generated molecular structures allows us to compare the MS data with the outcome of the algorithm. The species is said to be matched when its mass is represented by a peak in the spectrum and at least one reactant that makes the species is matched. The exact masses of each computationally-derived structure are calculated assuming the mass of only the most abundant isotope for each element. It is important to note that the model at this stage only provides the information on whether or not a species may be formed, hence, species concentrations are disregarded at this point. Explicit molecular structures of the monomers follow directly from the reaction network, while structures of the 'dimers' are reconstructed by combining species with one half crosslink of the same type. Radical species are not included in this comparison as they are not detected by MS. The calculated masses of reconstructed monomers and dimers are then adjusted using the exact masses of the possible ionizing ions for each mode, thus adding masses of H^+, Na^+ or NH_4^+ for positive mode and subtracting mass of H^- or adding mass of CH_3COO^- for negative mode.

The comparison of the calculated masses with the masses measured by ESI-MS of artificially aged EL is demonstrated in Fig. 6. The algorithm has identified 22 772 distinct structures in the measurement range of the instrument, out of which 7 756 were matched to the peaks of significant intensity, (that is peaks with intensity within 90% of top values in the spectrum). Many of distinct structures share the same molecular mass. Supplementary Table lists the molecular structures of all matched species.

In the mass spectra presented, measured peaks identified by calculation are coloured in blue, while those unidentified are orange. The height of the identified peak corresponds to the measured intensity in the MS spectrum. The results are displayed in the range from 50 to 850 m/z, which is sufficiently wide to capture the monomers and dimers. The peaks not identified with this procedure may correspond to
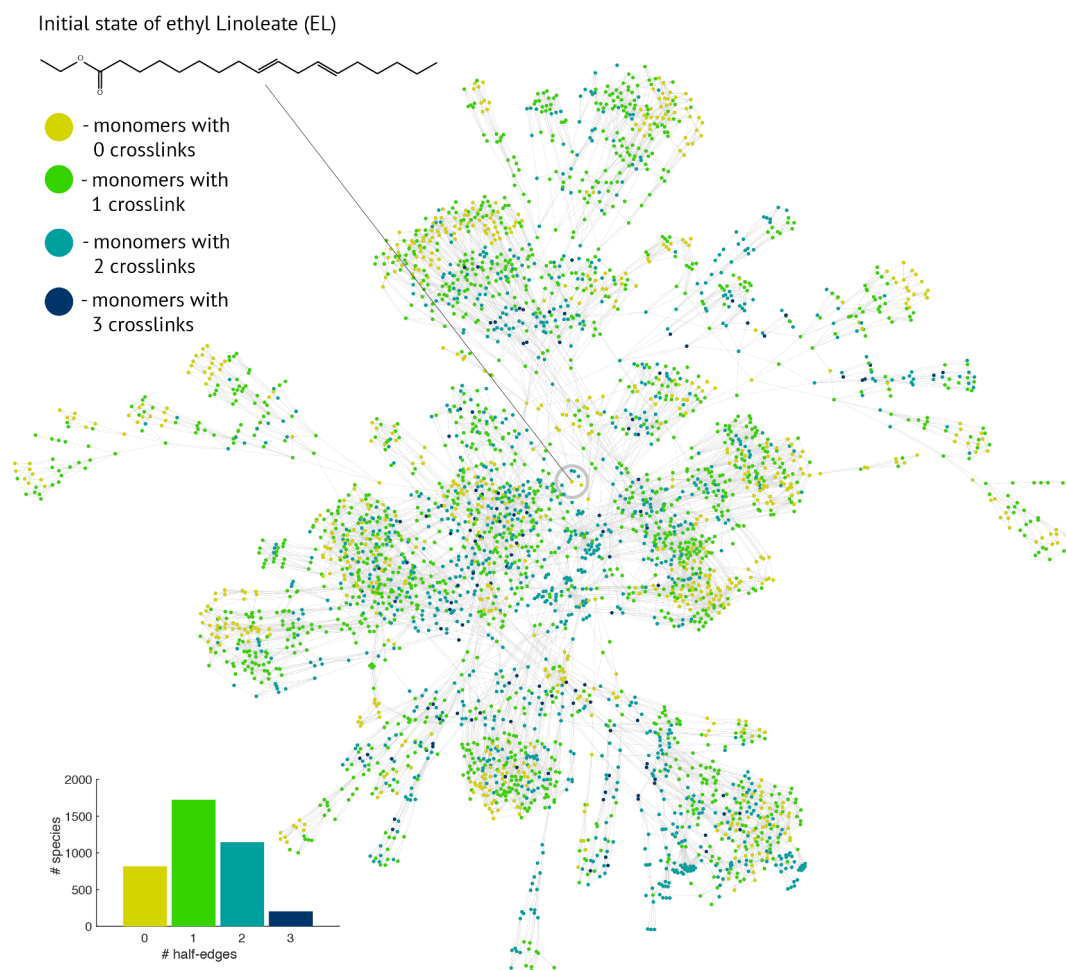
Fig. 5. Projected reaction network that describes the autoxidation of EL. The initial state of EL is highlighted and located in the middle of the reaction network. Nodes in this network correspond to the states of the monomers and the edges correspond to the transformation from a reactant to a product. As noted in the legend, colours of the nodes correspond to the number of half edges they bear, and the inset chart reports the total number of fragment species with 0,1,2,3. and 4 half-edges. (For interpretation of the references to colour in this figure legend, the reader is referred to the web version of this article.)

trimers and higher order oligomers formed by low molecular weight products, as well as to the products of the reaction pathways not included in the set of ARNG reaction rules, such as the epoxide ring opening reaction. The initial state of EL ($C_{20}H_{36}O_2 - H$) corresponds to the peak 307.15 m/z in negative mode, while the largest calculated masses of oxidized dimers correspond to 801.57 m/z in positive mode and 837.48 m/z in negative mode. Assignment of MS measured masses to specific chemical species is accompanied by the structural formulas of the matched molecules, see Supporting information for *MDL Molfiles*.

Knowing the identity of the majority of the peaks measured by MS allows us to determine the ranges of peaks produced by particular reaction pathways. General lipid polymerization is characterized by oxidation and crosslinking, which corresponds to the eventual formation of the insoluble fractions and secondary fragmentation (β scission), which breaks C–C bonds and releases lower molecular weight species from the polymer network [80]. Switching selected reactions on and off in the algorithm allows the determination of the regions of MS, where the products of oxidation, soluble crosslinked species (e.g. dimers) and β-scission are expected to appear (see Fig. 6). As the MS measurements are performed on the aged EL sample, products of β scission span most of the considered MS interval for both positive and negative modes indicating the degradation of polymer network [80].

3.3. Kinetic modeling

The reaction network for EL autoxidation directly yields a system of

3 887 nonlinear ODEs that describe the time evolution of concentrations of all (fragment) species. Reconstruction of a reaction network into a kinetic model is thoroughly described in [23]. The initial concentration of EL is 3.71 mol/L corresponding to 40 g of technical grade EL [45]. The concentration of the catalyst is 0.01 M, which corresponds to 0.07 wt.% Co(II) 2-ethylhexanoate (Co-EH). The choice of the catalyst is based on the availability of the detailed reaction mechanism of Co-EH and EL [49]. As diffusion of molecular oxygen is considered to be fast in comparison to the autoxidation process, its concentration is assumed to be constant: 2.18 mmol O_2/mol EL. All other species have their initial concentrations zero. These initial concentrations are in agreement with experimental measurements for soybean oil, which is representative for EL as it has high linoleic acid content [81,82].

The rate coefficients are estimated for each individual reaction using the Arrhenius equation. Pre-exponential factors are taken from literature, and the activation energy is estimated using the Evans-Polanyi approximation [58,60,69,70], see Methods for more details. In this work we disregard diffusion effects and assume that rate coefficients are constant over reaction time.

Starting with the initial concentrations and pre-calculated rate coefficients, the kinetic model is solved numerically using a semi-implicit multi-step integrator of 5th order (ode15s), assuming a reaction time of 1000 h as a realistic time span for drying of EL. The ODEs are solved in 8276 s for the model with drier and in 9301 s for the model without drier. The outcome of the simulation is the evolution of the concentrations of all species over the drying time. By aggregating these
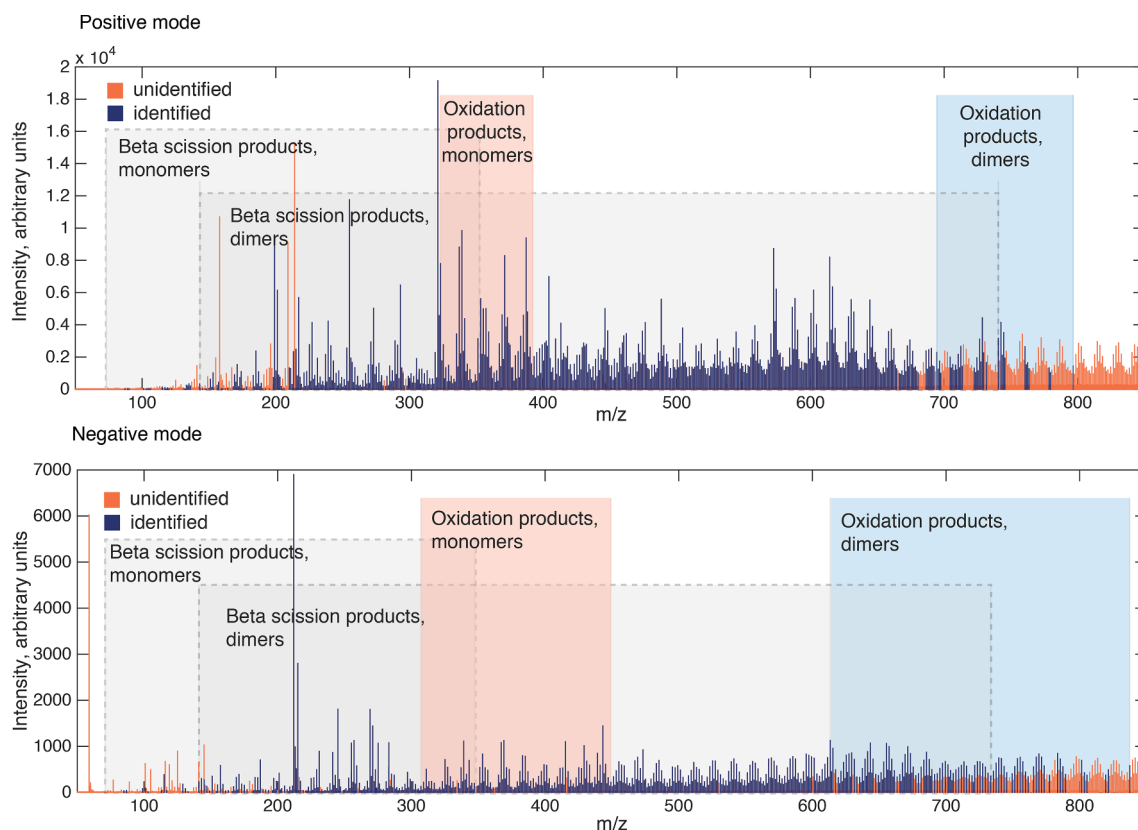
Fig. 6. Regions of mass spectra (both negative and positive mode) highlighting the anticipated products of oxidation and β-scission of monomers and dimers of EL. Peaks matched to the molecular structures generated by ARNG (dark blue) in the measured mass spectra (orange) of extracts from EL aged with titanium dioxide. Heights for matched peaks are set to the height of the corresponding measured peaks. (For interpretation of the references to colour in this figure legend, the reader is referred to the web version of this article.)

data according to the functional groups, we obtain the most important concentration profiles for oil drying: initial state of EL molecule, oxygen uptake, peroxide value, alcohols, double bonds, aldehydes, volatiles, carboxylic acid, radicals, crosslinks, and epoxides. Fig. 7 compares these data for the calculations with and without drier. Results for the system without drier are obtained by setting to zero the rate coefficients of the reactions between cobalt species and monomer states containing hydroperoxides. In no-drier mode, oxygen is assumed to play a role of the initiator. This assumption is based on the results of the work by Lazzari et al. [80], where the authors show that polymerization of oil happens in natural lab conditions without additives. The work by Pfaendtner and Broadbelt [69] suggests that the pre-exponential factor for this reaction is 10^{13} L/mol s and the activation energy equals to the heat of reaction. With this value of the pre-exponential factor, the solution of the kinetic model at the room temperature did not exhibit any observable changes in 1000 h, thus we investigated the behaviour of the system with higher values for this parameter. Appendix C demonstrates the sensitivity of concentration profiles to various values of pre-exponential factor of the initiation with oxygen. Starting form the value of 10^{17} L/mol s, we could observe changes in the system, and with the pre-exponential factor on the order of 10^{19} L/mol s the system demonstrated full consumption of EL in simulated time span of 1000 h. Thus, we used the latter value to obtain the results in Fig. 7 and demonstrate the difference in the behaviour of the system with and without drier.

The effect of the cobalt drier is visible in all concentration profiles shown in Fig. 7. An EL conversion of 50% is reached in 20 h without drier and in 3 h with drier. The drier significantly increases hydroperoxide decomposition causing a lower maximum of the hydroperoxide concentration profile. Fig. 7 also shows that the radical concentration in presence of drier is higher, which ultimately leads to a higher β-scission rate and consequently to higher carboxylic acid concentration. More

pronounced differences between drier and no-drier modes are observed in the formation of crosslinks and higher order oligomers. This result will be discussed in the following subsection.

The validity of the model can be assessed by analyzing the qualitative behaviour of various functional groups. The concentration decrease of EL is a marker for the overall progress of the polymerization process, while oxygen uptake is a measure of the rate. To quantify the oxygen uptake predicted by the model, the concentrations of all monomer states containing oxygen are summed up accounting for the number of added oxygen atoms per monomer. Experimental data for oxygen uptake is taken from work by Oyman et al. [45]. Oxygen uptake measurements are done in a stirred flask at room temperature in the presence of cobalt drier. The model predicts less oxygen uptake then the experimental measurements. This mismatch can be caused by the assumption made on the constant content of molecular oxygen in the system.

Hydroperoxides constitute an important intermediate product of the drying process of EL being formed via a reaction between carbon radicals and oxygen. Hydroperoxides are unstable species that over time decompose into alkoxy radicals and hydroxyl groups. Consequently, in the presence of drier, the concentration of hydroperoxides should pass through a maximum. A peak exists at around 20 h drying time, as is shown by the experimental profile from the work by Oyman et al. [45]. The model reproduces the maximum in the peroxide value much earlier, at around 1 h of drying time. The peroxide content was measured in a film, hence the discrepancy between modelled and experimental data may be due to the fact that the model does not account for diffusion effects, which may have a significant impact on the results. Peroxy crosslinks form another class of peroxide groups that can be formed during the drying process of EL. These crosslinks are formed via recombination between alkoxy or peroxy radicals, or via an addition
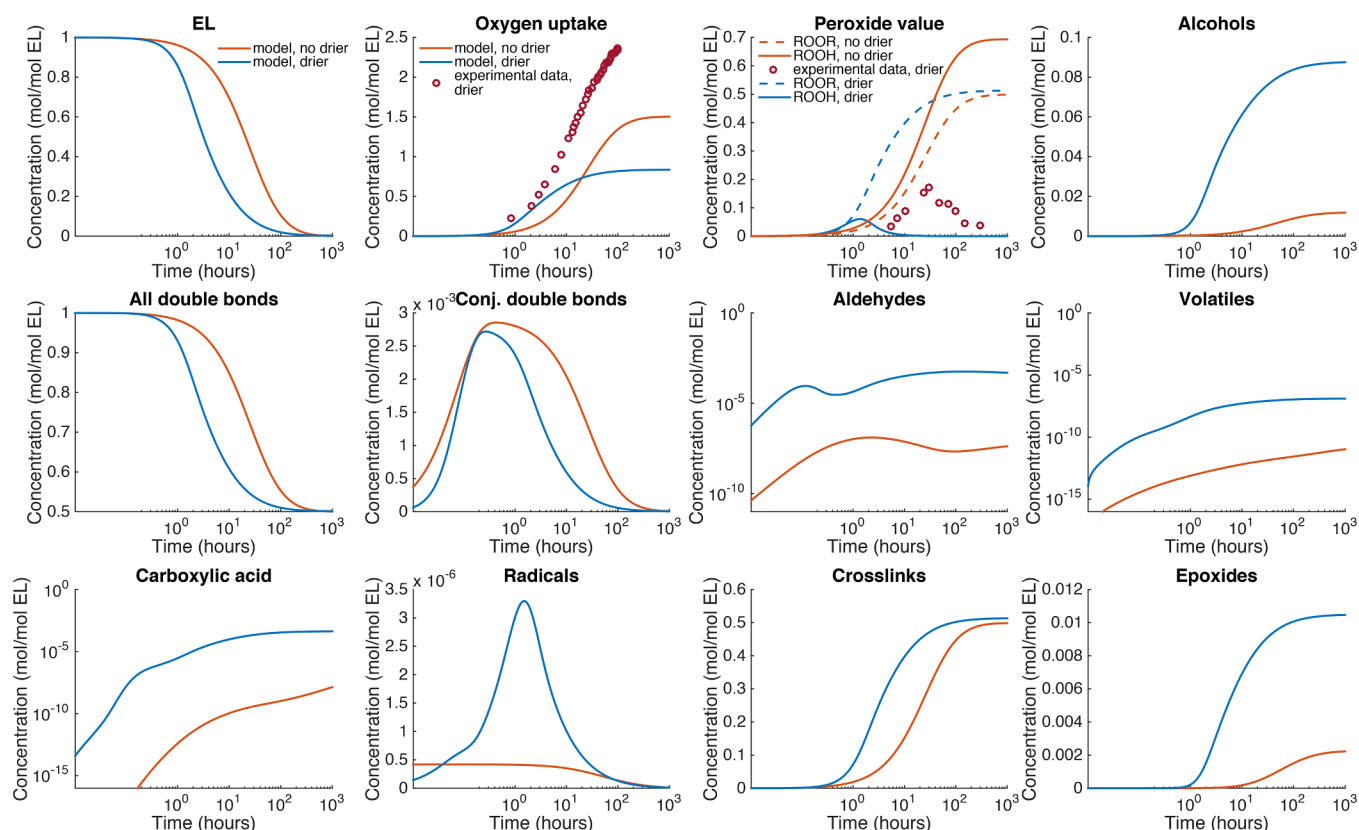
Fig. 7. Concentration profiles of various functional groups from the solution of the kinetic model for the case with drier and without drier.

reaction, where the peroxy radical attaches to a conjugated double bond. The behaviour of the concentration profile of peroxy crosslinks agrees with the observations in the experimental results [57,83], which report that peroxy crosslinks remain in the system even at late stages of drying.

The concentration profile of double bonds (C═C) as predicted by the model agrees with trends reported in experimental studies [45,80]. The concentration of species with *cis*-C═C (the initial state of EL) vanishes completely as EL is consumed, while conjugated double bonds are formed and subsequently consumed via an addition reaction. Thereafter, the concentration of all the remaining double bonds (*trans*-C═C) reaches a constant value, which, in our model, corresponds to 50% of the initial concentration of *cis*-C═C.

Alcohols are formed after hydroperoxide decomposition and remain in the system as end products [80]. Carboxylic acid is another type of end product that is formed after hydrogen abstraction from aldehydes. The transformation from aldehydes to carboxylic acid is noticeable in Fig. 8 in the concentration profiles predicted by the model at 75 °C, where the concentration of aldehydes starts decreasing and the amount of carboxylic acid increases significantly. The carboxylic acid content is particularly challenging to measure spectroscopically [84], so here the model serves to mitigate experimental limitations and to aid quantifying the amount of carboxylic acid in the system. Note that, with respect to carboxylic acid, that in the field of restoration and conservation of oil paintings, the presence of this oxidation product is an important marker of the condition of the painting as, interacting with metal pigments, it triggers the formation of metal soaps that are harmful to a painting [36]. Hexanal and pentanal have relatively low molecular weight and can leave the system as volatile compounds (causing the typical smell of drying oil paint). They are emitted in the beginning of

the drying process and then reach a constant concentration. The concentration of volatiles is under-predicted by the model as an experimentally reported concentration reaches the value of 2.5 mmol/mol EL after 30 h of drying [22]. Epoxides are formed via the reaction mechanism recently studied by Oakley et al. [58]. Several studies [57,83] observe epoxide decomposition occurring at late drying stages, however this reaction is not accounted for in the current work, as the reaction pathway is insufficiently known in the context of oil autoxidation and needs further exploration. The concentration of radicals remains small in the system. All radical species are formed and consumed within the drying time of 1000 h. The concentration of crosslinks reaches a constant value of 0.5 mol/mol EL, which implies that on average, each EL monomer takes part in the formation of one crosslink.

The concentration profiles of intermediate species, such as conjugated double bonds, radicals and hydroperoxides reveal that these species are consumed at late drying stage. Most reactions contribute to the formation of crosslinks, but the presence of alcohol, epoxide, aldehyde and carboxylic acid groups also indicates significant β-scission, as is shown by MS measurements.

Since we estimate the activation energies of all reactions, the kinetic model can be tested in different temperature regimes. Simulations of the drying process are performed for 5 temperatures in the range of 25–65 °C, as presented in Fig. 8 for the model in the presence of drier and in Appendix D for the model without drier. It is generally assumed that drying oil at temperatures less than 80 °C accelerates the autoxidation without introducing new reactions in the system [80]. The model seems to confirm this assumption, as the increase in temperature indeed leads to accelerated formation and decomposition of all functional groups, while concentration profiles for different temperature for most of the groups ultimately converge to the same steady state.
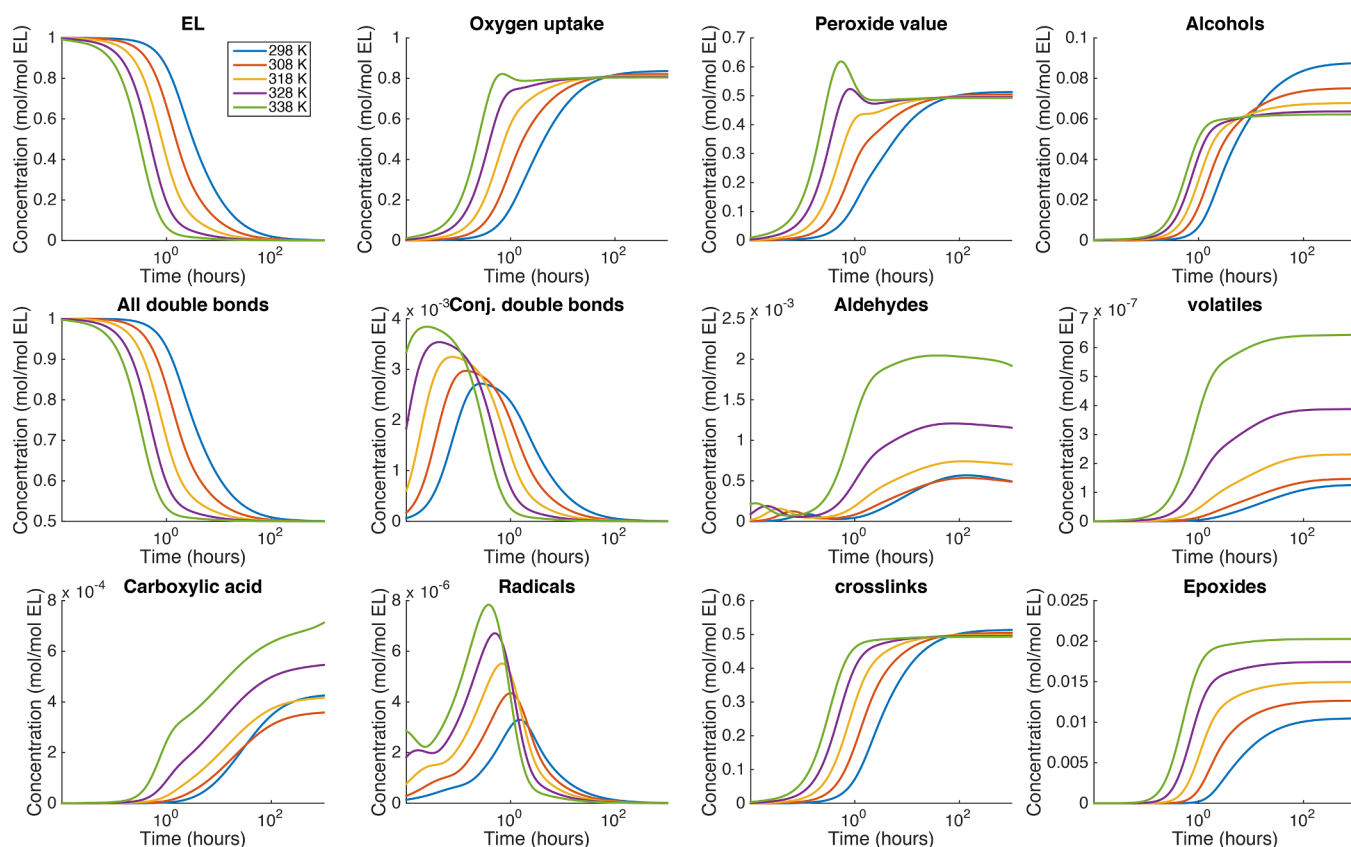
Fig. 8. Effects of different temperatures on the solution of the kinetic model with drier.
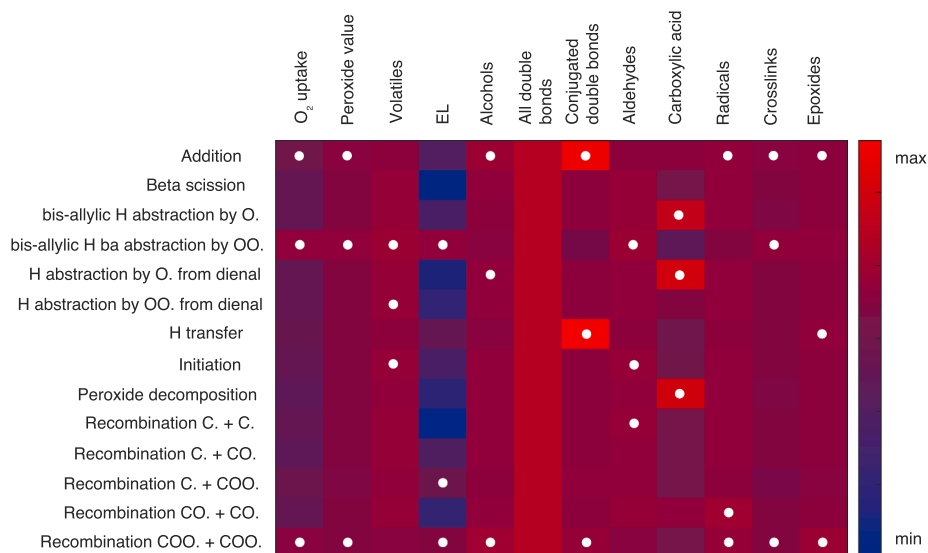
Fig. 9. Sensitivity results from varying pre-exponential factors of all reaction families presented as a heat-map. For each type of functional group, three highest sensitivities for different reactions are highlighted by the white dots.

Exceptions are formed by end products like alcohols and carboxylic acids. The steady-state concentration of alcohols at late drying stage decreases with the increase of temperature, whereas carboxylic acid content noticeably increases. This observation implies that with the increase of temperature alkoxy radicals are prone to undergo β-scission rather than hydrogen abstraction.

A major cause for the deviation between model and experimental results may be the fact that we were not able to sufficiently estimate the kinetic parameters. In other words, it is quite well possible that much better fits between model and data can be obtained with a different set of parameters. As a step towards efficient fitting of the rate parameters, we performed basic sensitivity analysis with the kinetic model, which in
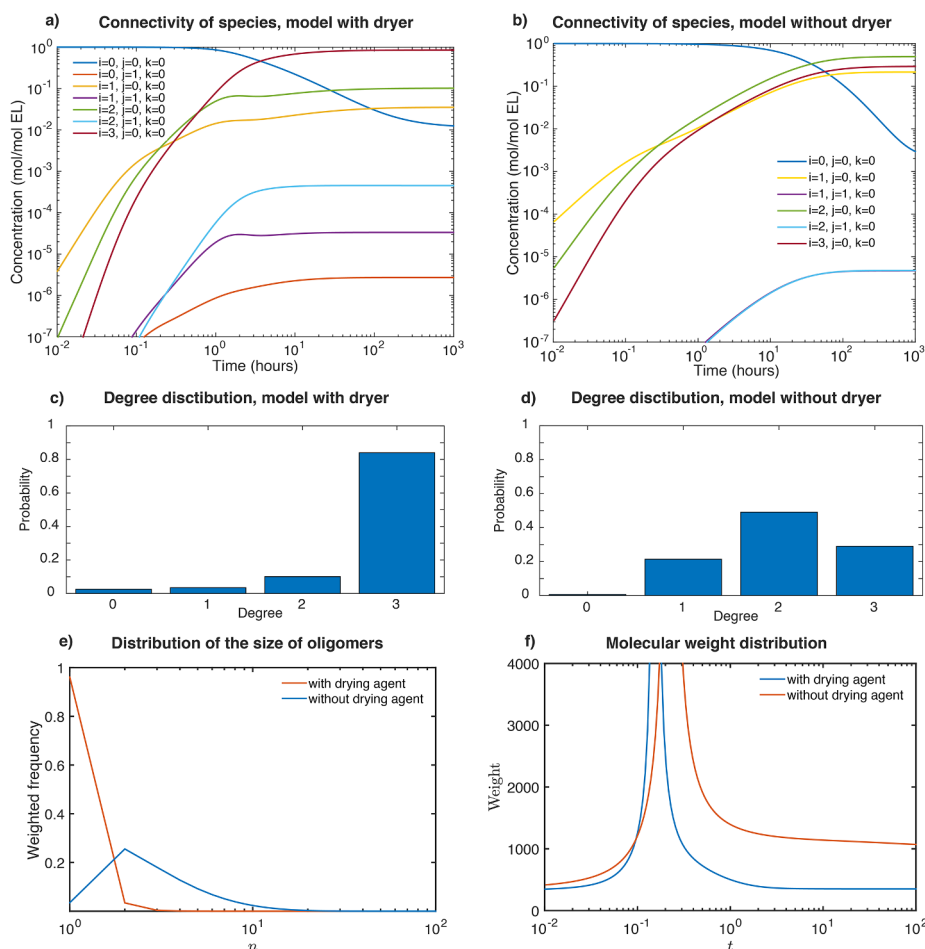
Fig. 10. (a, b) Relative fractions of fragments with different configurations of half crosslinks are plotted as a functions of time. Different types of crosslinks are distinguished: *i* stands for peroxy, *j* for ether, and *k* for alkyl. (c, d) – projected degree distribution at the steady state. The panels (a, c) on the left present results with drier, on the right (b, d) – without drier. (e) Weighted size distribution of oligomers in sol on the late stage of drying (at 1000 h); (f) average molecular weight of soluble fractions.

future may be expanded and lead to a model reduction [85]. The pre-exponential factors of all the reaction families were varied by several orders of magnitude and the cumulative response of various functional groups is represented as a heat-map in Fig. 9. The heat-map shows that consumption of EL and oxygen uptake are relatively insensitive to the kinetic parameters. For each functional group the three most sensitive reaction families are highlighted by a white dot. By counting the number of white dots in each row of the heat-map, one observes that the most influential reaction families are: addition, bis-allylic hydrogen abstraction by peroxy radical and recombination between peroxy radicals. This analysis confirms the expectation that the peroxy groups play a decisive role in the autoxidative drying processes.

3.4. Concentration of oligomers

Solving the ODE system associated to the reaction network of EL provides the concentration profiles of polymer constituents with their connections and of small species that do not belong to the polymer network. The random graph interpretation of such fragments allows discussing the macromolecular or global properties arising from the model for the oligomers, which are still finite in their size molecules (sol). It should be noted that the fragment species have sizes varying around the size of the EL monomer, depending on their oxidation state

and on whether or not they have undergone β-scission. Hence, there are significantly more different monomer units (namely, 3 887) than in most synthetic copolymers.

In addition to the heterogeneity of the monomer units there is also a variety of crosslinking types. EL monomers form up to three different crosslinks per monomer of three different types: alkyl, ether and peroxy. Fig. 10 a,b shows the concentration profiles of all chemically possible crosslink configurations per monomer for the cases with and without drier. Only the most probable configurations of crosslinks per monomer are included in the plot. Both plots demonstrate that the peroxy crosslink is the most abundant in the system.

The heterogeneity in monomer units and crosslink types makes it virtually impossible to arrive at two identical large polymer molecules, even when they are formed under the same conditions. In view of this fact, one should not regard exact instances of the structural polymer networks but rather the average properties of network ensembles – thus random graphs. For instance, one may characterize the 'size' of a polymer molecule by reporting the number of constituent fragment units, which can be directly derived from the degree distribution of the monomer units by using the properties of the underlying random graph [31]. Here, we will elucidate the variety of higher order oligomers' and finite polymer's properties that can be extracted from connectivity profiles.

Some units, see Fig. 4, bear half-edges (or half-crosslinks) that can be matched with half-edges of the same type sitting on other units, and therefore, one may generate a valid molecular structure by sequentially wiring a set of monomer nodes together. There are up to three half-edge per node in the case of EL. Such a combinatorial matching procedures are studied using random graphs [29,30,31,86–89]. Ref. [31] specifically addresses the implications of crosslinks of different types (colours) and provides analytical expressions for several quantities relevant in chemistry. Here, we answer questions about two of such chemically motivated quantities, namely: 1) What is the concentration of oligomer molecules consisting of a given number of nodes – the size distribution – at a given time point? and 2) How does average molecular size evolves in time as progressively larger macromolecular species appear during polymerization?.

We start with the evolution of the coloured degree distribution [31] as predicted by the model, see Fig. 10c, d, in the presence of drier and without it, and present the resulting macromolecular size distributions. It turns out that in presence of drier monomer units are dominantly appearing as three-functional nodes, whereas under no-drier conditions two-functional nodes are most abundant – a considerable difference in the *local* connectivity pattern. In both cases, the fraction of crosslinks is sufficient to achieve a highly connected network resulting in around 94% of the material being present as gel. However, the remarkable difference in the local connectivity pattern may suggest that the material might feature different physical and mechanical properties, such as elasticity [90].

Fig. 10e, d shows that indeed this difference has consequences for macromolecular properties: in presence of drier the size and molecular weight of soluble fractions is smaller and the time it takes to form a gel is shorter. On the late stage of drying, sol fraction in the presence of Co-EH consists mainly of dimers. The result is in agreement with the experimental data by Muizebelt et al. [91], where same conclusion is drawn for the long-term behaviour of EL in the presence of the same drying agent. Furthermore, apart from the intended acceleration of drying by adding drier – corresponding to shorter time to form gel – we observe two non-trivial effects: 1) drier permanently affects the structure of the polymer by making it more constrained, and 2) drier causes small polymer species not connected to gel to become even smaller and more prone to leave the system as volatiles. In relation to this finding we notice that due to the decomposition reactions (β-scission and peroxy crosslink decomposition), the model predicts that isolated monomers with no crosslinks ($i = 0, j = 0, k = 0$) should remain present in the system until the final state, amounting to about 5% of all fragments.

4. Conclusions

This paper demonstrates an *algorithmic* approach to modeling the complex polymerization process of a bio-based material which is a model system for the even more complex naturally drying oil, linseed oil. Formulating reaction networks of such systems algorithmically faces two major challenges: 1) heterogeneity of intermediate and product molecular species produced by the complex reaction mechanism; 2) growth of the polymers to unlimited sizes. The problem of modeling infinite-sized structures is addressed by using random graphs – the polymer network is represented as an annealed network, that is an ensemble of fragments bearing half crosslinks. Having explicit molecular structures of such fragments enables a comparison with mass spectra measured by ESI-MS. A wide range of experimentally measured masses are matched with molecular structures that contribute to the intensity of the corresponding peaks.

The complex polymerization problem addressed is represented by a large algorithmically formulated system of non linear ODEs. We report concentration profiles of various compounds and show that the oxygen uptake follows the same trend as observed in literature. The model also confirms the acceleration of the drying process in presence of cobalt drier and in higher temperature regimes. Moreover, the model at higher temperatures highlights the difference in the concentrations of the end products, such as alcohols and carboxylic acid. The results of the kinetic model complies with reported experimental data, although room for considerable improvement is foreseen by accurate estimation of the kinetic parameters, including diffusion control of reactions and more accurate experimental data. Sensitivity analysis revealed that the addition, bis-allylic hydrogen abstraction by peroxy radical, and peroxy radical recombination are the most influential reactions on the considered set of functional groups. Such sensitivity results may indicate which reaction families are worth considering in the parameter estimation procedure.

A major challenge for the developed model was to obtain the properties of higher order oligomers resulting from EL autoxidation. Using the ideas from random graphs, namely the coloured configuration model we were able to calculate the average molecular weight in the sol part of the system and weighted size distribution of finite polymer molecules, which is in line with experimental data.

An important next step in our modeling of EL is to find a method to reduce the large kinetic model to a size that allows parameter estimation. The reduction of the model to, for instance, a kinetic model of functional groups is impossible due to the nested nature of some of the reactive patterns. Additionally, uncertainty quantification is an important next step for such large systems involving numerous parameters. It is also necessary to include diffusion control in the model in view of the transition from liquid to solid taking place in the drying process. Furthermore, we will use the concept of fragment species to reconstruct kinetic models of larger molecules than EL, such as triglycerides. The methodology presented in this work is generic, and we expect it can be applied to model complex polymerization of many oils and hydrocarbons.

Declaration of Competing Interest

The authors declare that they have no known competing financial interests or personal relationships that could have appeared to influence the work reported in this paper.

Acknowledgements

Appendix A

Fig. 11.

Fig. 11. All patterns used to define the reaction scheme.

Appendix B

Reaction family	reaction
Co(III)OOR decomposition: [Co(III)OOR] $\rightarrow$ Co(II) + ROO	$R_{25} \rightarrow P_{23}$
	$R_{32} \rightarrow P_{24}$
Hydroperoxide decomposition: ROOH $\rightarrow$ RO. + HO.	$R_{10} \rightarrow P_3$
	$R_{31} \rightarrow P_{18}$
β-scission (see pathway 1 in Figure 1): RO. $\rightarrow$ RC(O)H + R.	$R_{17} \rightarrow P_4$
β-scission (see pathway 2 in Figure 1)	$R_{24} \rightarrow P_{15}$
Epoxidation from ROOH (see pathway 2 in Figure 1)	$R_{35} \rightarrow P_{19}$
	$R_{36} \rightarrow P_{19}$
Co(III)OOH $\rightarrow$ Co(II) + HO2.	$R_3 \rightarrow R_1$
Primary initiation:	
Co(II) + O2 $\rightarrow$ Co(III)OO.	$R_1 + R_4 \rightarrow R_2$
Oxidation: R. + O2 $\rightarrow$ ROO.	$R_8 + R_4 \rightarrow P_{10}$
	$R_{20} + R_4 \rightarrow R_{21}$
	$R_{19} + R_4 \rightarrow P_7$
	$R_{39} + R_4 \rightarrow P_{26}$
Secondary initiation: RH + Co(III)OO. $\rightarrow$ R. + Co(III)OOH	$R_2 + R_7 \rightarrow R_3 + P_1$
	$R_2 + R_7 \rightarrow R_3 + P_2$
Hydrogen abstraction: RH + ROO. $\rightarrow$ R. + ROOH	$R_9 + R_7 \rightarrow R_{10} + P_1$
	$R_9 + R_7 \rightarrow R_{10} + P_2$
	$R_{21} + R_7 \rightarrow R_{31} + P_1$
	$R_{21} + R_7 \rightarrow R_{31} + P_2$
Hydrogen abstraction: RH + RO. $\rightarrow$ R. + ROH	$R_{11} + R_7 \rightarrow R_{13} + P_1$
	$R_{11} + R_7 \rightarrow R_{13} + P_2$
	$R_{29} + R_7 \rightarrow R_{23} + P_1$
	$R_{29} + R_7 \rightarrow R_{23} + P_2$
ROOH decomposition with catalyst	
ROOH + Co(II) $\rightarrow$ RO. + [Co(III)OH-]	$R_{10} + R_1 \rightarrow R_{11} + R_5$
	$R_{31} + R_1 \rightarrow R_{29} + R_5$
Recombination: R. + R. $\rightarrow$ RR	$R_8 + R_8 \rightarrow P_{13} + P_{13}$
	$R_{19} + R_{19} \rightarrow P_8 + P_8$
	$R_{20} + R_8 \rightarrow R_{26} + P_{13}$
	$R_{20} + R_{19} \rightarrow R_{26} + P_8$
	$R_{20} + R_{20} \rightarrow R_{26} + R_{26}$
	$R_{19} + R_8 \rightarrow P_8 + P_{13}$
	$R_{39} + R_8 \rightarrow P_{27} + P_{13}$
	$R_{39} + R_{19} \rightarrow P_{27} + P_8$
	$R_{39} + R_{20} \rightarrow P_{27} + R_{26}$
Recombination:R. + ROO. $\rightarrow$ ROOR	$R_8 + R_9 \rightarrow P_{11} + R_{14}$
	$R_{19} + R_9 \rightarrow P_9 + R_{14}$
	$R_{20} + R_9 \rightarrow R_{27} + R_{14}$
	$R_{21} + R_8 \rightarrow R_{27} + P_{11}$
	$R_{21} + R_{19} \rightarrow R_{27} + P_9$
	$R_{21} + R_{20} \rightarrow R_{27} + R_{27}$
	$R_{39} + R_9 \rightarrow P_{28} + R_{14}$
	$R_{39} + R_{21} \rightarrow P_{28} + R_{27}$
Recombination:RO. + RO. $\rightarrow$ ROOR	$R_{11} + R_{11} \rightarrow R_{14} + R_{14}$
	$R_{29} + R_{11} \rightarrow R_{27} + R_{14}$
	$R_{29} + R_{29} \rightarrow R_{27} + R_{27}$
#	reaction
Recombination:R. + RO. $\rightarrow$ ROR	$R_{11} + R_8 \rightarrow R_{15} + P_{12}$
	$R_{19} + R_{11} \rightarrow P_{14} + R_{15}$
	$R_{20} + R_{11} \rightarrow R_{28} + R_{15}$
	$R_{29} + R_8 \rightarrow R_{28} + P_{12}$
	$R_{29} + R_{19} \rightarrow R_{28} + P_{14}$
	$R_{29} + R_{20} \rightarrow R_{28} + R_{28}$
	$R_{39} + R_{11} \rightarrow P_{29} + R_{15}$
	$R_{39} + R_{29} \rightarrow P_{29} + R_{28}$
Hydrogen abstraction: RC(O)H + ROO. $\rightarrow$ RC(O). + ROOH	$R_{18} + R_9 \rightarrow R_{20} + R_{10}$
	$R_{18} + R_{21} \rightarrow R_{20} + R_{31}$
Hydrogen abstraction: RC(O)H + RO. $\rightarrow$ RC(O). + ROH	$R_{18} + R_{11} \rightarrow R_{20} + R_{13}$
	$R_{18} + R_{29} \rightarrow R_{20} + R_{23}$
Bayer Villiger:RC(O)OOH + RC(O)H $\rightarrow$ 2RC(O)OH	$R_{22} + R_{18} \rightarrow R_{23} + P_6$
ROOH + [Co(III)OH-] $\rightarrow$ [Co(III)OOR] + H$_2$O	$R_{10} + R_5 \rightarrow R_{25} + R_6$
	$R_{31} + R_5 \rightarrow R_{32} + R_6$
ROOR decomposition: ROOR $\rightarrow$ RO. + RO.	$R_{14} + R_{14} \rightarrow P_{30} + P_{30}$
	$R_{27} + R_{27} \rightarrow P_{31} + P_{31}$
	$R_{27} + R_{14} \rightarrow P_{31} + P_{30}$
Addition (see Figure 1)	$R_9 + R_{12} \rightarrow R_{14} + R_{33}$
	$R_9 + R_{12} \rightarrow R_{14} + R_{34}$
Epoxidation from ROOR (see pathway 1 in Figure 1)	$R_{33} + R_{14} \rightarrow P_{32} + P_{30}$
	$R_{34} + R_{14} \rightarrow P_{32} + P_{30}$

Hydrogen transfer: RH + R. → R. + RH	$R_8 + R_7 \rightarrow P_{33} + P_1$
	$R_8 + R_7 \rightarrow P_{33} + P_2$
	$R_{19} + R_7 \rightarrow P_{34} + P_1$
	$R_{19} + R_7 \rightarrow P_{34} + P_2$
	$R_{20} + R_7 \rightarrow R_{18} + P_1$
	$R_{20} + R_7 \rightarrow R_{18} + P_2$
Recombination:ROO. + ROO. → ROOR + O2	$R_9 + R_9 \rightarrow R_{14} + R_{14} + R_4$
	$R_{21} + R_9 \rightarrow R_{27} + R_{14} + R_4$
	$R_{21} + R_{21} \rightarrow R_{27} + R_{27} + R_4$
[Co(III)OOR] + ROOH → [Co(III)OOR, HOOR] → RO. + [Co(III)OOR,OH]	
[Co(III)OOR,OH] → ROO. + [Co(III)OH-]	$R_{25} + R_{10} \rightarrow R_{11} + R_9 + R_5$
	$R_{25} + R_{31} \rightarrow R_{11} + R_{21} + R_5$
	$R_{32} + R_{10} \rightarrow R_{29} + R_9 + R_5$
	$R_{32} + R_{31} \rightarrow R_{29} + R_{21} + R_5$
Russell termination:ROO. + ROO. → ROH + R(O) + O2	$R_{30} + R_{30} \rightarrow P_{21} + P_{22} + R_4$

Reaction rules formalising the chemical reactions on the level of reactive (R_i) and nonreactive (P_i) patterns, as defined in Table 1.
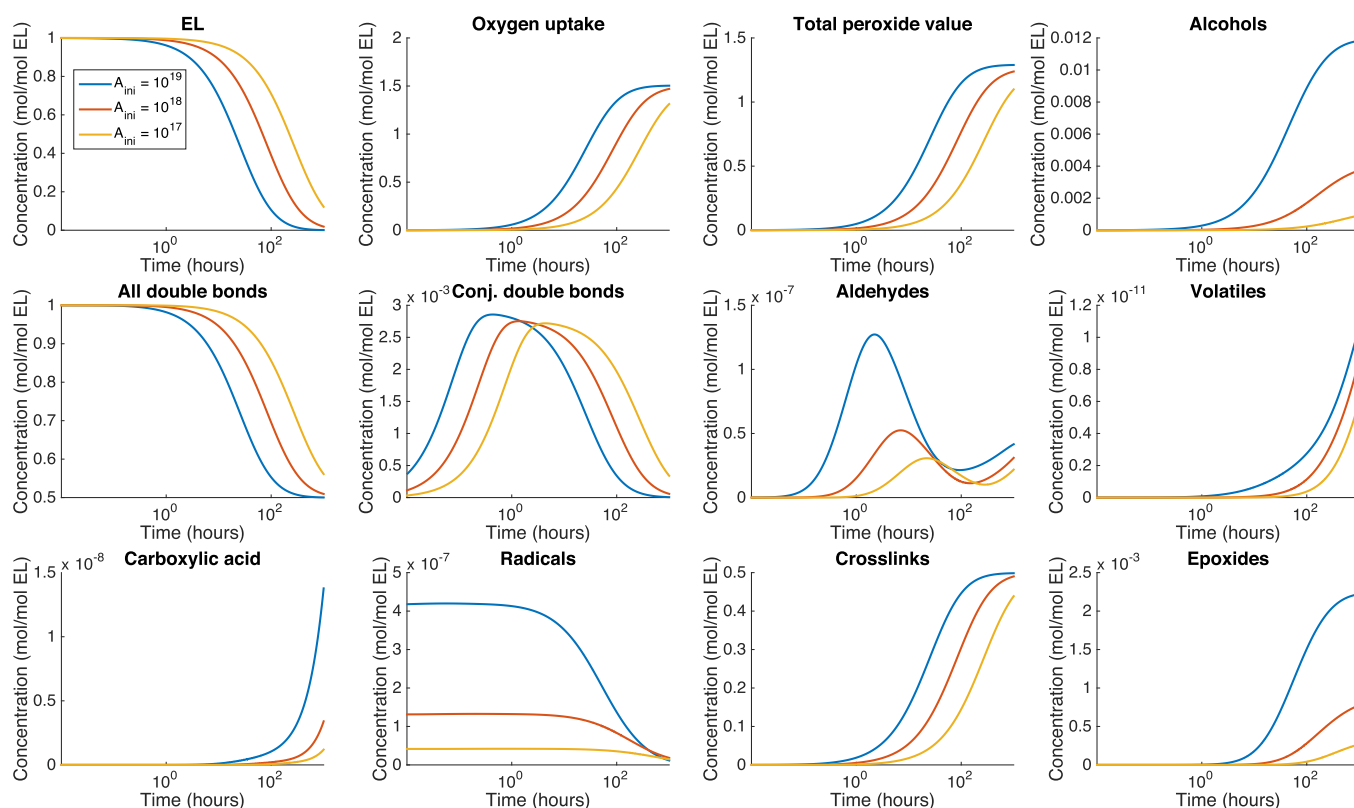
Appendix C

Fig. 12.

Fig. 12. Concentration profiles of various functional groups from the solution of the kinetic model for the case without drier with various pre-exponential factors of the initiation with oxygen.
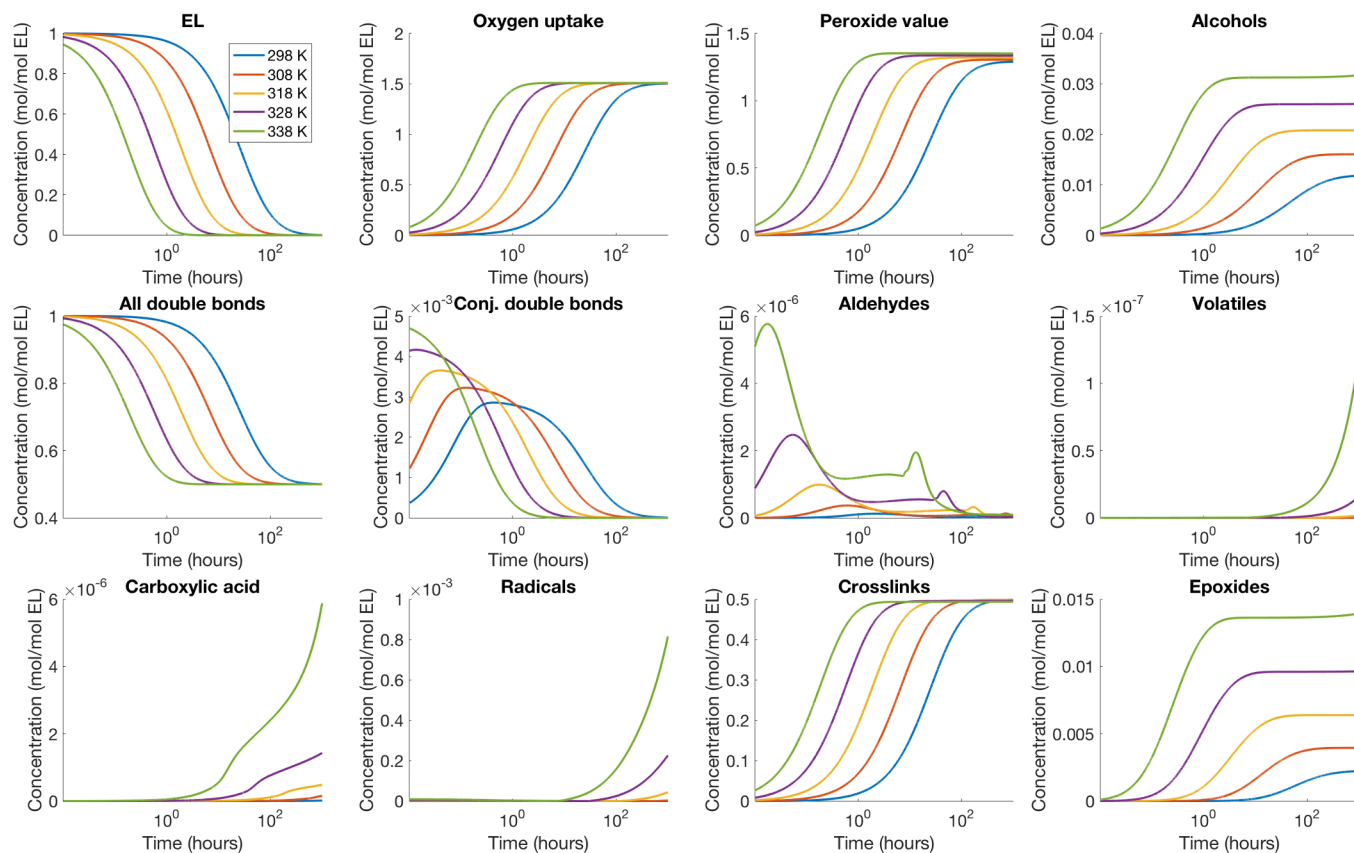
Appendix D

Fig. 13.

Fig. 13. Effects of different temperatures on the solution of the kinetic model without drier.

Appendix E. Supplementary data

Supplementary data associated with this article can be found, in the online version, at https://doi.org/10.1016/j.cej.2020.126485.

References

[1] Stephen Hanessian, Jonathan Franco, Benoit Larouche, The psychobiological basis of heuristic synthesis planning-man, machine and the chiron approach, Pure Appl. Chem. 62 (10) (1990) 1887–1910.

[2] Orr Ravitz, Data-driven computer aided synthesis design, Drug Discov. Today: Technol. 10 (3) (2013) e443–e449.

[3] Yukio Yoneda, A computer program package for the analysis, creation, and estimation of generalized reactions–grace. i. Generation of elementary reaction network in radical reactions–grace(i), Bull. Chem. Soc. Jpn. 52 (1) (1979) 8–14.

[4] P.J. Clymans, G.F. Froment, Computer-generation of reaction paths and rate equations in the thermal cracking of normal and branched paraffins, Comput. Chem. Eng. 8 (2) (1984) 137–142.

[5] Linda J. Broadbelt, Scott M. Stark, Michael T. Klein, Computer generated pyrolysis modeling: on-the-fly generation of species, reactions, and rates, Ind. Eng. Chem. Res. 33 (4) (1994) 790–799.

[6] E. Ranzi, T. Faravelli, P. Gaffuri, A. Sogaro, Low-temperature combustion: automatic generation of primary oxidation reactions and lumping procedures, Combust. Flame 102 (1–2) (1995) 179–192.

[7] Frédérique Battin-Leclerc, Development of kinetic models for the formation and degradation of unsaturated hydrocarbons at high temperature, Phys. Chem. Chem. Phys. 4 (2002) 2072–2078.

[8] Nick M. Vandewiele, Kevin M. Van Geem, Marie-Françoise Reyniers, Guy B. Marin, Genesys: kinetic model construction using chemo-informatics, Chem. Eng. J. 207–208 (2012) 526–538.

[9] Jing Song, Building robust chemical reaction mechanisms: next generation of automatic model construction software (Ph.D. thesis), Massachusetts Institute of Technology, 2004.

[10] Srinivas Rangarajan, Aditya Bhan, Prodromos Daoutidis, Language-oriented rule-based reaction network generation and analysis: Description of ring, Comput. Chem. Eng. 45 (2012) 114–123.

[11] Connie W. Gao, Joshua W. Allen, William H. Green, Richard H. West, Reaction mechanism generator: automatic construction of chemical kinetic mechanisms, Comput. Phys. Commun. 203 (2016) 212–225.

[12] H. Jeong, B. Tombor, R. Albert, Z.N. Oltvai, A.-L. Barabási, The large-scale organization of metabolic networks, Nature 407 (2000) 651–654.

[13] Jorg Stelling, Steffen Klamt, Katja Bettenbrock, Stefan Schuster, Ernst Dieter Gilles, Metabolic network structure determines key aspects of functionality and regulation, Nature 420 (2002) 190–193.

[14] Dmitry Yu Zubarev, Dmitrij Rappoport, Alán Aspuru-Guzik, Uncertainty of prebiotic scenarios: The case of the non-enzymatic reverse tricarboxylic acid cycle, Scientific Rep. 5 (2015).

[15] Marlies Nijemeisland, Loai K.E.A. Abdelmohsen, Wilhelm T.S. Huck, Daniela A. Wilson, Jan C.M. van Hest, A compartmentalized out–of–equilibrium enzymatic reaction network for sustained autonomous movement, ACS Cent. Sci. 2 (2016) 843–849.

[16] H. Jeong, S.P. Mason, A.-L. Barabási, Z.N. Oltvai, Lethality and centrality in protein networks, Nature 411 (2001) 41–42.

[17] Eugen Lounkine, Michael J. Keiser, Steven Whitebread, Dmitri Mikhailov, Jacques Hamon, Jeremy L. Jenkins, Paul Lavan, Eckhard Weber, Allison K. Doak, Serge Côté, Brian K. Shoichet, Laszlo Urban, Large-scale prediction and testing of drug activity on side-effect targets, Nature 486 (2012) 361–367.

[18] Guy Shinar, Martin Feinberg, Structural sources of robustness in biochemical reaction networks, Science 5971 (327) (2010) 1389–1391.

[19] M. Grom, G. Stavber, P. Drnovsek, B. Likozar, Modelling chemical kinetics of a complex reaction network of active pharmaceutical ingredient (api) synthesis with process optimization for benzazepine heterocyclic compound, Chem. Eng. J. 283

(2016) 703–716.

[20] I. Otero-Muras, P. Yordanov, J. Stelling, Chemical reaction network theory elucidates sources of multistability in interferon signaling, PLOS Com. Boil. 13(4) (2017).

[21] Lindsay H. Oakley, Francesca Casadio, Kenneth R. Shull, Linda J. Broadbelt, Microkinetic modeling of the autoxidative curing of an alkyd and oil-based paint model system, Appl. Phys. A 121 (3) (2015) 869–878.

[22] Lindsay H. Oakley, Francesca Casadio, Professor Kenneth R. Shull, Professor Linda J. Broadbelt, Modeling the evolution of crosslinked and extractable material in an oil-based paint model system, Angew. Chem. Int. Ed. 57(25) (2018) 7413–7417.

[23] Yuliia Orlova, Ivan Kryven, Piet D. Iedema, Automated reaction generation for polymer networks, Comput. Chem. Eng. 112 (2018) 37–47.

[24] P.D. Iedema, N.H. Kolhapure, Mathematical Methods, Wiley-VCH Verlag GmbH, 2008, pp. 431–532.

[25] Hidetaka Tobita, Archie E. Hamielec, Polymerization Processes, 2. Modeling of Processes and Reactors, Wiley-VCH Verlag GmbH & Co, KGaA, 2000.

[26] Vahid Vajihinejad, J.B.P. Soares, Monitoring polymer flocculation in oil sands tailings: a population balance model approach, Chem. Eng. J. 346 (2018) 447–457.

[27] Ivan Kryven, Jorien Duivenvoorden, Joen Hermans, Piet D. Iedema, Random graph approach to multifunctional molecular networks, Macromol. Theory Simul. 25 (5) (2016) 449–465.

[28] Verena Schamboeck, Ivan Kryven, Pieter D. Iedema, Acrylate network formation by free-radical polymerization modeled using random graphs, Macromol. Theory Simul. (2017) 1700047.

[29] Ivan Kryven, Analytic results on the polymerisation random graph model, J. Math. Chem. (Aug 2017).

[30] Ivan Kryven, General expression for the component size distribution in infinite configuration networks, Phys. Rev. E 95 (May 2017) 052303 .

[31] Ivan Kryven, Bond percolation in coloured and multiplex networks, Nat. Commun. 10 (404) (2019).

[32] Ilaria Bonaduce, Leslie Carlyle, Maria Perla Colombini, Celia Duce, Carlo Ferrari, Erika Ribechini, Paola Selleri, and Maria Rosaria Tiné, New insights into the ageing of linseed oil paint binder: a qualitative and quantitative analytical study, PLoS ONE 7(11) (2012).

[33] Maria Perla Colombini, Francesca Modugno, Marina Giacomelli, Sandro Francesconi, Characterisation of proteinaceous binders and drying oils in wall painting samples by gas chromatography – mass spectrometry, J. Chromatogr. A 846 (1) (1999) 113–124.

[34] Yuliia Orlova, Alessa A. Gambardella, Ivan Kryven, Katrien Keune, Piet D. Iedema, Algorithmic discovery of reaction steps interprets mass spectra of triolein.

[35] Katrien Keune, Jennifer Mass, Apurva Mehta, Jonathan Church, Florian Meirer, Analytical imaging studies of the migration of degraded orpiment, realgar, and emerald green pigments in historic paintings and related conservation issues, Heritage Sci. 4 (10) (2016).

[36] Joen J. Hermans, Katrien Keune, Annelies van Loon, Piet D. Iedema, The crystallization of metal soaps and fatty acids in oil paint model systems, Phys. Chem. Chem. Phys. 18 (2016) 10896–10905.

[37] Lambert Baij, Joen J. Hermans, Katrien Keune, Piet Iedema, Time-dependent atr-ftir spectroscopic studies on fatty acid diffusion and the formation of metal soaps in oil paint model systems, Angew. Chem. Int. Ed. 57 (25) (2018) 7351–7354.

[38] Stefan Michalski, A physical model of the cleaning of oil paint, Stud. Conserv. 35 (sup1) (1990) 85–92.

[39] Alan Phenix, Ken Sutherland, The cleaning of paintings: effects of organic solvents on oil paint films, Stud. Conserv. 46 (sup1) (2001) 47–60.

[40] David Erhardt, Charles S. Tumosa, Marion F. Mecklenburg, Long-term chemical and physical processes in oil paint films, Stud. Conserv. 50 (2) (2005) 143–150.

[41] Raymond J. Meilunas, James G. Bentsen, Arthur Steinberg, Analysis of aged paint binders by ftir spectroscopy, Stud. Conserv. 35 (1) (1990) 33–51.

[42] Jacky Mallégol, Jacques Lemaire, Jean-Luc Gardette, Drier influence on the curing of linseed oils, Prog. Org. Coat. 39 (2000) 107–113.

[43] Jacky Mallégol, Jean-Luc Gardette, Jacques Lemaire, Long-term behavior of oil-based varnishes and paints i. spectroscopic analysis of curing drying oils, JAOCS 76 (8) (1999) 967–976.

[44] Z. Okan Oyman, W. Ming, R. van der Linde, Oxidation of model compound emulsions for alkyd paints under the influence of cobalt drier, Prog. Org. Coat. 48 (2003) 80–91.

[45] Z.O. Oyman, W. Ming, R. van der Linde, R. van Gorkum, E. Bouwman, Effect of [mn (acac)3] and its combination with 2,2'-bipyridine on the autoxidation and oligomerisation of ethyl linoleate, Polymer 46 (2005) 1731–1738.

[46] Remy van Gorkum, Elisabeth Bouwman, The oxidative drying of alkyd paint catalysed by metal complexes, Coord. Chem. Rev. 249 (2005) 1709–1728.

[47] Elisabeth Bouwman, Remy van Gorkum, A study of new manganese complexes as potential driers for alkyd paints, J. Coat. Technol. Res. 4 (4) (2007) 491–503.

[48] Jacky Mallégol, Jean-Luc Gardette, Jacques Lemaire, Long-term behavior of oil-based varnishes and paints. photo- and thermooxidation of cured linseed oil, JAOCS 77 (3) (2000) 257–263.

[49] Eyal Spier, Ulrich Neuenschwander, Ive Hermans, Insights into the cobalt(ii)-catalyzed decomposition of peroxide, Angew. Chem. Int. Ed. 52 (2013) 1581–1585.

[50] M.D. Soucek, T. Khattab, J. Wu, Review of autoxidation and driers, Prog. Org. Coat. 73 (2012) 435–454.

[51] Juita, Bogdan Z. Dlugogorski, Eric M. Kennedy, John C. Mackie, Low temperature oxidation of linseed oil: a review, Fire Sci. Rev. 1(3) (2012).

[52] Jan Honzíček, Curing of air-drying paints: a critical review, Ind. Eng. Chem. Res. 58 (28) (2019) 12485–12505.

[53] Huiyong Yin, Ned A. Porter, New insights regarding the autoxidation of polyunsaturated fatty acids, Antioxid. Redox Signal. 7 (1–2) (2005) 170–184.

[54] Huiyong Yin, Libin Xu, Ned A. Porter, Free radical lipid peroxidation: mechanisms and analysis, Chem. Rev. 111 (10) (2011) 5944–5972.

[55] Ned A Porter, Sarah E Caldwell, Karen A Mills, Mechanisms of free radical oxidation of unsaturated lipids, Lipids 30 (4) (1995) 277–290.

[56] Ned A. Porter, Bruce A. Weber, Hugo Weenen, Jamil A. Khan, Autoxidation of polyunsaturated lipids. Factors controlling the stereochemistry of product hydroperoxides, J. Am. Chem. Soc. 102 (17) (1980) 5597–5601.

[57] W.J. Muizebelt, J.J. Donkerbroek, M.W.F. Nielen, J.B. Hussem, M.E.F. Biemond, R.P. Kloosen, K.H. Zabel, Oxidative crosslinking of alkyd resins studied with mass spectrometry and nmr using model compounds, J. Coat. Technol. 70 (876) (1998) 80–91.

[58] Lindsay H. Oakley, Francesca Casadio, Kenneth R. Shull, Linda J. Broadbelt, Theoretical study of epoxidation reactions relevant to hydrocarbon oxidation, Ind. Eng. Chem. Res. 56 (2017) 7454–7461.

[59] Pär Fjällström, Barbro Andersson, Calle Nilsson, Kurt Andersson, Drying of linseed oil paints: a laboratory study of aldehyde emissions, Ind. Crops Prod. 16 (2002) 173–184.

[60] Lindsay H. Oakley, Francesca Casadio, Kenneth R. Shull, Linda J. Broadbelt, Examination of mechanisms for formation of volatile aldehydes from oxidation of oil-based systems, Ind. Eng. Chem. Res. 57 (1) (2018) 139–149.

[61] Gregor N. Simm, Alain C. Vaucher, Markus Reiher, Exploration of reaction pathways and chemical transformation networks, J. Phys. Chem. A 123 (2) (2019) 385–399.

[62] Linda J. Broadbelt, Scott M. Stark, Michael T. Klein, Computer generated pyrolysis modeling: on-the-fly generation of species, reactions, and rates, Ind. Eng. Chem. Res. 33 (4) (1994) 790–799.

[63] Subhash C. Basak, Sharon Bertelsen, Gregory D. Grunwald, Application of graph theoretical parameters in quantifying molecular similarity and structure-activity relationships, J. Chem. Inf. Comput. Sci. 34 (1994) 270–276.

[64] Edward S. Blurock, Computer-aided synthesis design at risc-linz: automatic extraction and use of reaction classes, J. Chem. Inf. Comput. Sci. 30 (4) (1990) 505–510.

[65] Connor W. Coley, William H. Green, Klavs F. Jensen, Machine learning in computer-aided synthesis planning, Acc. Chem. Res. 51 (5) (2018) 1281–1289.

[66] A. Nigam, M.T. Klein, A mechanism-oriented lumping strategy for heavy hydrocarbon pyrolysis: Imposition of quantitative structure-reactivity relationships for pure components, Ind. Eng. Chem. Res. (United States) 32 (7) (1993) 7.

[67] Linda J. Broadbelt, Jim Pfaendtner, Lexicography of kinetic modeling of complex reaction networks, AIChE J. 51 (8) (2005) 2112–2121.

[68] M.G. Evans, M. Polanyi, Inertia and driving force of chemical reactions, Trans. Faraday Soc. 34 (1938) 11–24.

[69] Jim Pfaendtner, Linda J. Broadbelt, Mechanistic modeling of lubricant degradation. 1. Structure-reactivity relationships for free-radical oxidation, Ind. Eng. Chem. Res. 47 (2008) 2886–2896.

[70] Jim Pfaendtner, Linda J. Broadbelt, Mechanistic modeling of lubricant degradation. 2. The autoxidation of decane and octane, Ind. Eng. Chem. Res. 47 (2008) 2897–2904.

[71] R. Vinu, Linda J. Broadbelt, Unraveling reaction pathways and specifying reaction kinetics for complex systems, Annu. Rev. Chem. Biomol. Eng. 3 (2012) 29–54.

[72] Sidney W Benson, Thermochemical Kinetics: Methods for the Estimation of Thermochemical Data and Rate Parameters, Wiley, New York, NY, 1968.

[73] Maarten K. Sabbe, Mark Saeys, Marie-Françoise Reyniers, Guy B. Marin, Veronique Van Speybroeck, Michel Waroquier, Group additive values for the gas phase standard enthalpy of formation of hydrocarbons and hydrocarbon radicals, J. Phys. Chem. A 109 (33) (2005) 7466–7480.

[74] Paschalis D. Paraskevas, Maarten K. Sabbe, Marie-Françoise Reyniers, Nikos Papayannakos, Guy B. Marin, Group additive values for the gas-phase standard enthalpy of formation, entropy and heat capacity of oxygenates, Chem. A Eur. J. 19 (48) (2013) 16431–16452.

[75] Shumaila S. Khan, Xinrui Yu, Jeffrey R. Wade, R. Dean Malmgren, Linda J. Broadbelt, Thermochemistry of radicals and molecules relevant to atmospheric chemistry: Determination of group additivity values using g3//b3lyp theory, J. Phys. Chem. A 113 (17) (2009) 5176–5194.

[76] C. Franklin Goldsmith, Gregory R. Magoon, William H. Green, Database of small molecule thermochemistry for combustion, J. Phys. Chem. A 116 (2012) 9033–9057.

[77] N. Cohen, Revised group additivity values for enthalpies of formation (at 298 k) of carbon-hydrogen and carbon-hydrogen-oxygen compounds, J. Phys. Chem. Ref. Data 25 (6) (1996) 1411–1481.

[78] B.A. van Driel, K.J. van den Berg, M. Smout, N. Dekker, P.J. Kooyman, J. Dik, Investigating the effect of artists' paint formulation on degradation rates of tio2-based oil paints, Heritage Sci. 6 (21) (2018).

[79] Johannes T. Margraf, Karsten Reuter, Systematic enumeration of elementary reaction steps in surface catalysis, ACS Omega 4 (2) (2019) 3370–3379.

[80] Massimo Lazzari, Oscar Chiantore, Drying and oxidative degradation of linseed oil, Polym. Degrad. Stab. 65 (2) (1999) 303–313.

[81] Eunok Choe, David B. Min, Mechanisms and factors for edible oil oxidation, Comprehens. Rev. in Food Sci. Food Saf. 5 (4) (2006) 169–186.

[82] F.D. Gunstone, F.B. Padley, Lipid Technologies and Applications, CRC Press, 2018.

[83] W.J. Muizebelt, J.C. Hubert, R.A.M. Venderbosch, Mechanistic study of drying of alkyd resins using ethyl linoleate as a model substance, Prog. Org. Coat. 24 (1) (1994) 263–279.

[84] Lambert Baij, Louise Chassouant, Joen J. Hermans, Katrien Keune, Piet D. Iedema, The concentration and origins of carboxylic acid groups in oil paint, RSC Adv. 9 (2019) 35559–35564.

[85] Zoltán Till, Tamás Varga, János Sója, Norbert Miskolczi, Tibor Chován, Reduction

of lumped reaction networks based on global sensitivity analysis, Chem. Eng. J. 375 (2019) 121920 .

[86] Ivan Kryven, Finite connected components in infinite directed and multiplex networks with arbitrary degree distributions, Phys. Rev. E 96 (2017) 052304 .

[87] Ivan Kryven, Emergence of the giant weak component in directed random graphs with arbitrary degree distributions, Phys. Rev. E 94 (1) (2016) 012315 .

[88] Verena Schamboeck, Piet D. Iedema, Ivan Kryven, Dynamic networks that drive the process of irreversible step-growth polymerization, Scientific Rep. 9 (1) (2019) 1–18.

[89] Verena Schamboeck, Ivan Kryven, Piet D Iedema, Effect of volume growth on the percolation threshold in random directed acyclic graphs with a given degree distribution, Phys. Rev. E 101 (1) (2020) 012303 .

[90] W.J. Muizebelt, J.C. Hubert, R.A.M. Venderbosch, A.J.H. Lansbergen, R.P. Klaasen, K.H. Zabel, Aluminum compounds as additional crosslinkers for air-drying high-solids alkyd paints, J. Coat. Technol. 70 (882) (1998) 53–59.

[91] W.J. Muizebelt, M.W.F. Nielen, Oxidative crosslinking of unsaturated fatty acids studied with mass spectrometry, J. Mass Spectrom. 31 (5) (1996) 545–554.